Development of tools for the study of AIP56 binding/translocation domain

José Martinho Oliveira Peres

Mestrado em Bioquímica

Departamento de Química e Bioquímica

2014

Orientador

Doutora Ana do Vale, Investigadora auxiliar, IBMC

Coorientadores

Dr.ª Marisa Pereira, Estudante de doutoramento, IBMC

Doutora Rute Pinto, Investigadora de pós-doutoramento,IBMC

IBMC INEB
Laboratório Associado . Associate Laboratory

U.PORTO

INSTITUTO DE CIÊNCIAS BIOMÉDICAS ABEL SALAZAR
UNIVERSIDADE DO PORTO

U.PORTO

FACULDADE DE CIÊNCIAS
UNIVERSIDADE DO PORTO

Todas ascorreções determinadas pelo júri, e só essas, foram efetuadas.
O Presidente do Júri,

Porto, _____/_____/_____

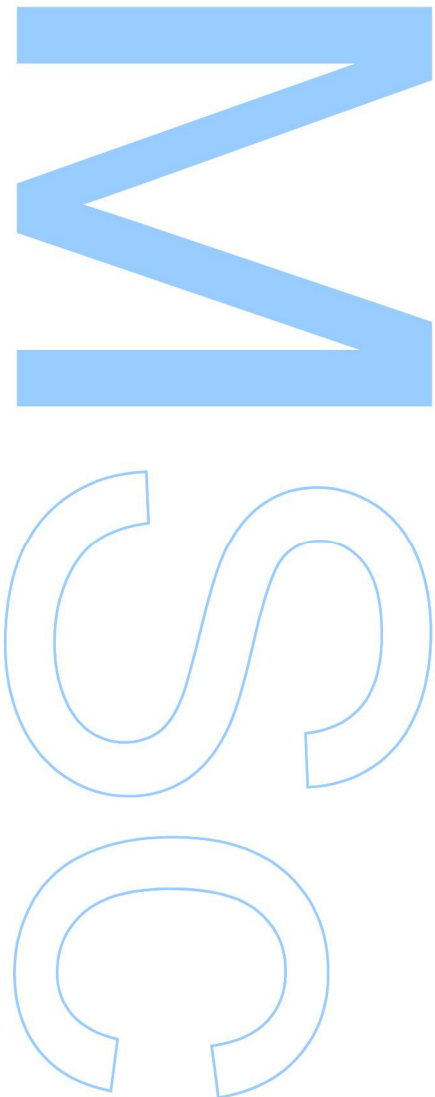

Agradecimentos

Gostaria de agradecer a todas as pessoas, nomeadamente colegas de trabalho, amigos e familiares, que me ajudaram e me apoiaram durante toda esta jornada.

Um especial agradecimento à Doutora Ana do Vale pela oportunidade e orientação; à Rute e à Marisa pelos ensinamentos, apoio e conselhos (essenciais durante todo o projeto); à Inês pelos conselhos e partilhase aos meus amigos pela paciência e pela alegria que me transmitiram.

Um sentido e sincero muito obrigado

Abstract

AIP56 (apoptosis-inducing protein of 56 kDa) is a major virulence factor of *Photobacterium damselae piscicida* (*Phdp*), a Gram-negative bacterium that causes septicemic infections in several marine fish species with great economic importance in mariculture worldwide. This bacterial toxin belongs to the AB family, a group of protein toxins that exert their functions at the host cells' cytosol. In order to reach the cytosol, the catalytic domain of these toxins must be delivered by their carrier domain after specific interaction with receptors on the surface of target cells and consequent internalization. Upon *Phdp* infections, AIP56 induces macrophages and neutrophils death through an apoptotic process that, *in vivo*, culminates in secondary necrosis of these cells. These events contribute to the necrotic lesions observed in the diseased animals. Although the toxic effects of AIP56 and their contribution to the pathology of *Phdp* infections have already been disclosed, the structural determinants of the toxin required for different steps of the intoxication process remain to be identified.

The work herein presented provides important tools for the study of region(s) involved in the binding/translocation of AIP56 into the cytosol of target cells. More specifically, six chimeric proteins, consisting in different AIP56 C-terminal truncates fused with two distinct reporter moieties (β-lactamase and diphtheria toxin catalytic domain) were designed for this purpose. DNA sequences encoding these proteins were obtained using molecular biology methods and the expression of the chimeras was performed in *Escherichia coli*. This was followed by the purification of recombinant proteins through affinity chromatography. Lastly, the catalytic activity of each protein, conferred by their respective moiety, was tested and confirmed by specific enzymatic assays. With this final step completed, the enzymatically active chimeras produced in this project can now be used in *in vivo* tests to further enhance our knowledge about the structural organization of AIP56 and to disclose important aspects of the binding/translocation mechanism of this AB toxin. It is expected that a more extensive understanding of the toxin's structural features, intracellular pathways and molecular mechanisms of action will allow the use of AIP56 as a tool in cell biology and even in medical sciences, as a potential therapeutic agent.

Keywords: *Photobacterium damselae piscicida*; AIP56; AB toxin; intoxication; domain organization

Resumo

AIP56 (*apoptosis-inducing protein of 56 kDa*) é um factor de virulência importante da *Photobacterium damselae piscicida* (*Phdp*), uma bactéria Gram-negativa que causa septicémias em muitas espécies de peixes com grande importância económica em aquacultura em todo o mundo. Esta toxina bacteriana pertence à família de toxinas AB, um grupo de toxinas proteicas que exercem as suas funções no citosol das células hospedeiras. De modo a alcançar o citosol, o domínio catalítico destas toxinas deve ser entregue pelo seu domínio de transporte, o que acontece após interação específica com recetores na superfície das células alvo e consequente internalização. Durante infeções por *Phdp*, a AIP56 induz a morte de macrófagos e neutrófilos por um processo apoptótico que, *in vivo*, culmina na necrose secundária destas células. Estes eventos contribuem para as lesões necróticas observadas em animais doentes. Embora os efeitos tóxicos da AIP56 e a sua contribuição para a patologia das infecções causadas por *Phdp* já tenham sido revelados, os determinantes estruturais da toxina necessários para os diferentes passos do processo de intoxicação ainda permanecem por descobrir.

O trabalho aqui apresentado fornece ferramentas importantes para o estudo da região (ou regiões) envolvidas na ligação/translocação da AIP56 para o citosol das células-alvo. Mais especificamente, seis proteínas quiméricas, consistindo em diferentes truncados C-terminal da AIP56 fundidos com duas porções repórter distintas (β-lactamase e o domínio catalítico da toxina da difteria) foram criadas para este propósito. As sequências de ADN codificantes para estas proteínas foram obtidas usando métodos de biologia molecular e a expressão das quimeras foi realizada em *Escherichia coli*. Seguiu-se a purificação das proteínas recombinantes por cromatografia de afinidade. Por fim, a actividade catalítica de cada proteína, conferida pela respectiva porção repórter, foi testada e confirmada por ensaios enzimáticos específicos. Com este passo final completo, as quimeras produzidas neste projecto podem ser agora usadas em testes *in vivo* para enriquecer ainda mais o nosso conhecimento sobre os determinantes estruturais da AIP56 e para revelar aspetos importantes do mecanismo de ligação/translocação desta toxina AB. É espectável que um conhecimento mais aprofundado das características estruturais da toxina, das vias intracelulares e dos mecanismos moleculares de ação irá permitir o uso da AIP56 como ferramenta em biologia celular e até em ciências médicas, como potencial agente terapêutico.

Palavras-chave: *Photobacteriumdamselaepiscicida*; AIP56; toxina AB; intoxicação; organização estrutural

Table of contents

List of tables and figures

List of abbreviations

ADP	Adenosine diphosphate
AIP56	Apoptosis-inducing protein of 56 kDa
BoNT	Botulinum neurotoxin
cAMP	Cyclic adenosine monophosphate
CNTs	Clostridial neurotoxins
Ctx	Cholera toxin
CTB	Ctx B subunit
DMEM	Dulbecco's modified essential medium
DNA	Deoxyribonucleic acid
dNTP	Deoxynucleotide triphosphate
DT	Diphtheria toxin
Dta	DT catalytic domain
DTT	Ditiotreitol
EDTA	Ethylenediaminetetraacetic acid
EF-2	Elongation factor 2
ER	Endoplasmic reticulum
FBS	Fetal bovine serum
GLB	Gel loading buffer
GM1	Monosialotetrahexosylganglioside
hb-EG	Heparin binding epidermal growth factor precursor
HBSS	Hank's balanced salt solution
HC	Heavy chain
IPTG	Isopropyl-β-D-thiogalactopyranoside
LC	Light chain
LCCM	L929 cell-conditioned media
mBMDM	Mouse bone marrow derived macrophages
NAD^+	Aldehyde dehydrogenase
NF-κB	Nuclear factor-κB
PA	Protective antigen
PCR	Polymerase chain reaction
PDI	Proteindisulfide isomerase
PGA	poly-γ-glutamic acid
Phdp	*Photobacteriumdamselaepiscicida*

Ptx Pertussis toxin

RNA Ribonucleic acid

RT Room temperature

SDS-PAGE Sodium dodecyl sulfate - polyacrylamide gel electrophoresis

SNARE Soluble N-ethylmaleimide-sensitive factor attachment protein receptor

SOC Super Optimal broth medium with Catabolite repression

Stx Shiga toxin

TBS Tris-buffered saline

TeNT Tetanus neurotoxin

TGN *trans*-Golgi network

T-TBS Tris-buffered saline containing 0.1% Tween 20

X-GAL 5-bromo-4-chloro-3-indolyl-beta-D-galacto-pyranoside

Chapter I:
Introduction

A. Bacterial toxins

During infection of the host, bacterial pathogens often produce macromolecular substances with enzymatic properties. The purpose of these macromolecules is to improve proliferation and survivability of bacteria with limited capacity to disseminate in the host through either impairment of physiological functions or infliction of damage into the host tissues. Since the discovery and isolation of the diphtheria toxin, in 1888, by Emile Roux and Alexandre Yersin [1], these compounds have been designated as toxins and their study has proven to be vital to understand the pathogenicity mechanisms used by several infectious agents.

At a chemical level, these toxins can be divided into two major classes: endotoxins, which are comprised of toxic lipopolysaccharide components of the outer membrane of Gram-negative bacteria, and exotoxins, which are protein toxins [2].

Endotoxins are mostly located on the surface of the outer membrane of Gram-negative bacteria cell walls and they are secured to this cellular structure by ionic and hydrophobic forces[2].

Unlike the endotoxins, the majority of exotoxins are secreted by bacteria and often act distanced from the site of infection [3]. Based on their site of action, exotoxins can be divided into two groups: toxins that act on the cell's plasma membrane and toxins that act in the cytosol [4]. The first group can either act as host receptor agonists or antagonists (interfering and causing impairment of the signal transduction pathways) or by forming pores that lead to the disruption of the membrane integrity [5]. In contrast, the second group exerts their enzymatic functions against specific cytosolic targets, after reaching the cytosol either by receptor-mediated endocytosis and subsequent translocation across the membrane of an intracellular compartment, or by direct delivery through bacteria injection systems [5].

Many of the toxins that act intracellularly are physically organized into distinct domains that play different functional roles: recognition of receptors on the surface of sensitive host cells, internalization of the toxin itself, and enzymatic activity towards specific intracellular components of the host cells [5].

B. AB toxins

A well-known group of cytosol-orientated exotoxins acting at the host cells' cytosol exert their functions by delivering their toxic enzymatic components into host cells after specific interaction with receptors on the surface of these cells and consequent internalization [5]. These toxins can be functionally described as molecular syringes, mostly due to their intrinsic ability to translocate the catalytic domain into the cytosol, and they are more commonly known as AB toxins [5]. This group

encompasses toxins such as diphtheria toxin (DT) and Shiga toxin (Stx), which target the cell translational machinery, tetanus neurotoxin (TeNT) and botulinum neurotoxin (BoNT), which target SNARE (soluble N-ethylmaleimide-sensitive factor attachment protein receptor)machinery (important for the fusion of neurotransmitters vesicles and consequent exocytosis), and cholera toxin (Ctx) which increases the second messenger cyclic adenosine monophosphate (cAMP) [5].

Throughout the last few decades, the study of AB toxins has revealed an increasing and remarkable therapeutic potential for these toxic proteins in several areas of interest [6]. AB toxins are successfully used as antigens in vaccines. Examples of this application are the vaccines against diphtheria, tetanus, and whopping cough (DTPa). These vaccines are based on DT, TeNT and pertussis toxoids, respectively, and are administrated to the population as part of the national vaccination program [7]. Anthrax toxin, whose protective antigen (PA) subunit was shown to induce protection against lethal doses of this toxin, in guinea pigs, when conjugated with poly-γ-glutamic acid (PGA) capsule peptide, is another example of an AB toxin applied as antigen [6].

AB toxins also show an incredible potential as adjuvants of the immune response or, alternatively, as suppressors of autoimmunity [6]. For instance, in early studies, Ctx B subunit (CTB) coupled with specific auto-antigens was shown to induce a state of immunological tolerance, providing improved protection of mice against several autoimmune diseases [6]. In addition, due to their catalytic functions and cell binding specificities, these toxins can also be exploited in the treatment of cancer in the form of immunotoxins. These chimeric proteins are composed of a targeting moiety, which usually is a monoclonal antibody or a recombinant protein that displays the ability to bind to a specific and high affinity receptor, and the effector moiety of a bacterial toxin. A successful example of these fusion proteins is DAB_{389}IL-2 (ONTAK®) which was approved in 1999 for the treatment of CD25 positive refractory cutaneous T cell lymphoma and it has the ability to direct the DT catalytic domain (DTa) to cells that express the high affinity IL-2 receptor [8]. This type of approach has also been developed based on other AB toxins, namely *Pseudomonas* exotoxin A and ricin toxin, among others [9].

1. Structural organization

In general terms, AB toxins comprise two functional components: an effector component (also designated as A subunit) and a carrier component (also known as B subunit). The A subunit is usually an enzyme or a factor, responsible for the toxin's enzymatic activity, that employs its specific function through intracellular protein-protein interactions. On the other hand, the B subunit possesses a specific receptor-binding function and is responsible for the internalization and delivery of the toxin into the host cell's cytosol [10]. These two domains can be linked by disulfide bonds or associated by non-covalent interactions [6].

Most of AB toxins are synthesized and secreted from their producing bacteria as an inactive

single-chain polypeptide [11, 12]. This inactive precursor can be activated by proteolysis mediated by the producing organism (e.g. Ctx, ricin, clostridial neurotoxins) or by target cells' proteases, usually furin (e.g. DT, Stx, *Pseudomonas* exotoxin A), that act in an exposed region between two cysteine residues [12]. Proteolytic cleavage often results in di-chain toxin molecules linked by a disulfide bond [11, 12].

Even though the majority of AB toxins are produced in a single-chain form, some of these toxins are comprised of independently synthesized A and B subunits that are assembled afterwards by non-covalent bonds in order to yield a final multimeric toxin [6]. Generally, these complexes are formed by a single A subunit linked to a B pentamer (AB_5), like pertussis toxin (Ptx) and Ctx[13]or by multiple A subunits bound to heptameric (AB_7) or octameric (AB_8) oligomers of B-subunits, like the anthrax toxin [14]. Recently, a new A_2B_5 organization was unveiled for*Salmonella*Typhi typhoid toxin[8]. This arrangement is comprised of two covalently linked A subunits associated to a pentameric B subunit by non-covalent interactions.

2. Intoxicationmechanism

The most common mechanism of action of AB toxins comprises four steps that lead to the transport of the toxin from the extracellular space into the interior of the host cell, where the A domain displays its specific enzymatic activity towards a selected cytosolic protein [15]. The first step of this process is the specific binding of the B subunit of the toxin to its host cell receptor [15]. This is followed by endocytosis of the AB toxin into an intracellular compartment. Thirdly, toxins undergo conformational changes which consequently lead to the translocation of the A subunit into the cytoplasm. Finally, the A subunit reaches the cytosol, interacts with its host cell target and performs its function (figure 1) [15].

Although the intoxication mechanism described above is common to the majority of AB toxins, the mode of internalization varies from toxin to toxin. Based on their way of entering into the cytosol, AB toxins can be divided into two main groups: toxins that reach the cytosol from the acidic endosomal compartment, and toxins that translocate to the cytosol from the endoplasmic reticulum (ER) [12, 16]. In both cases, it is presumed that the interchain disulfide bound that links A and B domains must be reduced in order to allow release the A moiety into the cytosol [11].

Toxins like anthrax toxin, DT, AIP56 and clostridial neurotoxins (CNTs) are internalized into early endosomes, where acidification of the endosomal lumen by a vesicular ATPase [17, 18]triggers conformational changes on the B domain [17]. This event enables it to penetrate the lipid bilayer and form a channel/pore on the endosomal membrane through which the unfolded form of A subunit can cross into cytosol. When it reaches the cytosol, it refolds due to the neutral pH of this compartment [11, 15].

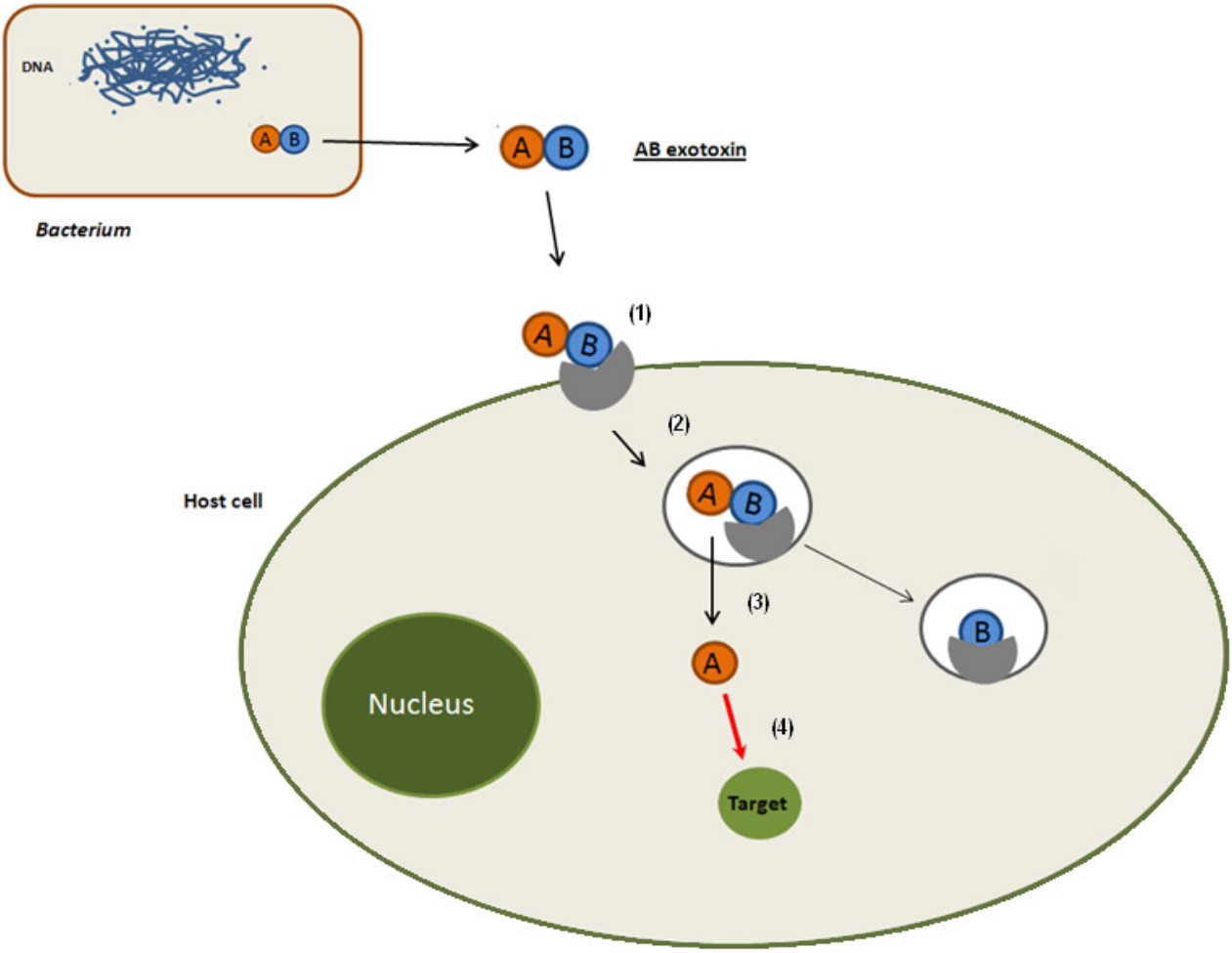

Figure 1 – Schematic picture of the general mechanism of cell intoxication conducted by AB toxins. (1) Cell binding by interaction of B domain with a specific surface receptor. (2) Internalization via endocytosis of the toxin. (3) Translocation of the catalytic A domain across the vesicle membrane into the cytosol. (4) Enzymatic activity of A subunit towards a specific cytosolic target [15]

In contrast, toxins such as Stx, Ctx and Pseudomonas exotoxin A, undergo retrograde transport through the Golgi complex in order to reach the ER from where the A moiety is released into the cytosol [11]. In both intracellular trafficking pathways, it is presumed that the interchain disulfide bound that links A and B domains must be reduced during translocation of A moiety into the cytosol in order to release this component [11].

Despite all the facts already known there is still plenty of unveiled information about AB toxins cytosolic translocation that urges for further studies.

3. Diphtheria toxin

DT is one of the most extensively studied and well understood bacterial toxin [19]. Its use as a model system has provided, throughout the decades, key insights for the analysis of other protein toxins intoxication processes[8].

Synthesized by toxigenic strains of *Corynebacteriumdiphtheria*e, the causative agent of the diphtheria disease, this AB toxin is released into the culture medium as a 535 amino acid single-chain protein after cleavage of its 25 amino acid signal peptide[20]. DT is comprised of two fragments: fragment A, which contains the catalytic DTa domain, and fragment B, which is composed of the receptor binding (R) and translocation (T) domains [8]. The DTa domain catalyzes the ADP-ribosylation of elongation factor 2 (EF-2), by ADP (adenosine diphosphate) moiety transfer from NAD^+ (aldehyde dehydrogenase), leading to the inhibition of cellular protein synthesis and ultimately to cell death by apoptosis [8, 21]. The ADP-ribosyltransferase activity of DT is activated by proteolytic nicking in an exposed 14 amino acid loop flanked by two cysteine residues that form a disulfide bond[8]. The binding of the toxin to its cell surface receptor, a heparin binding epidermal growth factor precursor (hb-EGF) is mediated by the R-domain[8, 22], while the T-domain is involved in the translocation of the C-domain into the cytosol [8].

DT follows the general AB toxin intoxication mechanism. It firstly binds to its membrane anchored cell receptor, and afterwards, receptor bound toxin is concentrated in clathrin coated pits and internalized into clathrin coated vesicles, which are then converted into early endossomes vesicles[23]. The next step involves acidification of these compartments by a vacuolar ATPase, which lowers the luminal pH. This process triggers the dynamic unfolding of DT, allowing the insertion into the vesicle membrane and formation of a cation-selective pore through which the unfolded catalytic domain translocates into the cytosol [8]. Translocation of DTa is followed by reduction of the disulfide bound between the A and B fragments, resulting in the release of the DTa domain. Once in the cytosol, a refolding process generates an enzymatically active form of the DTa domain, which mediates the NAD^+-dependent ADP ribosylation of EF-2 [24].

4. Cholera toxin

Ctx, a member of the AB_5 family of toxins, is secreted by the gram-negative bacterium *Vibrio cholerae,* the causative agent of cholera disease[25]. This bacterial toxinis comprised of six polypeptides: one catalytic subunit (A), formed by an enzymatically active A1-chain and an A2-chain, and five identical B subunits assembled non-covalently into a ring-shaped stable homopentamer [25]. Prior to secretion, the A subunit links, in a non-covalent way, to the B subunit, an interaction mediated by the A2-chain that results in the formation of the holotoxin [25]. The A1 chain of the A subunit acts as an ADP-ribosyltransferase that modifies the heterotrimeric G protein, Gsα, leading to the constitutive modification of adenylate cyclase and the rapid production of cAMP[25]. In contrast, B subunit is responsible for the binding of the toxin to target cells by interaction with the ganglioside GM1 (monosialotetrahexosylganglioside) found in plasma membrane microdomains (lipid rafts) [26].

Ctx intoxication process begins with the binding to the ganglioside GM1, which transports the

toxin throughout the secretory pathway from the plasma membrane to the ER. Due to the ring-like pentameric structure of the B subunit, five GM1 molecules can be clustered at once. The clustering likely increases the efficiency of retrogade trafficking to the ER [25]. Endocytosis of the toxin complex from the plasma membrane to early endosomes can occur by various mechanisms involving clathrin- and caveolin-dependent and independent mechanisms, and is followed by traffic of the toxin to early and recycling endosomes [25]. Afterwards, the toxin complex travels from the early endosomes to the trans-Golgi network (TGN) through a process not fully understood, which is believed to be independent of the late endosomal pathway [25]. Once at the TGN, CT-GM1 complex might bypass the Golgi cisternae, trafficking directly to the ER [27]. Upon entering the ER, the A1-chain is recognized and unfolded by the reduced form of the chaperone protein disulfide isomerase (PDI). The PDI-A1-chain complex is then presumably targeted to a protein on the lumenal membrane of the ER, where PDI is oxidized by the ER oxidase in order to induce the release of the A1-chain [25]. Afterwards, the unfolded A1-chain is transferred across the ER membrane into the cytosol by an unclear retro-translocation process. Unlike most retro-translocation substrates, the A1-chain escapes degradation by the proteasome and refolds in the cytosol to perform its enzymatic function against Gsα [25].

5. Clostridial neurotoxins

The CNTs are produced by species of anaerobic, Gram-positive, spore-forming, rod-shaped, bacteria within the genus *Clostridium*[5].This subfamily of AB toxins includes toxins such as TeNT and BoNT, two of the most toxic proteins for humans, but also commonly used in the therapy of many human neurological disorders and cosmetic production[28].

CNTs are synthesized as single polypeptide chains, which are post-translationally cleaved by bacterial and tissue proteases. This cleavage yields a light chain (LC) and a heavy chain (HC) that remain covalently and reversibly linked by a disulfide bond until being exposed to reducing conditions within the neuronal cytosol [28]. The HC mediates neuronal cell surface binding, internalization by receptor-mediated endocytosis, and transport of the LC across the membrane into the cytosol, while the LC is responsible for the catalytic activity of the neurotoxin [28].

In order to intoxicate peripheral nerve cells, CNTs first need to selectively bind to complex gangliosides, a class of glycosphingolipids that are particularly abundant in the outer leaflet of nerve cell membranes. This interaction promotes the accumulation, on the plasma membrane, of the neurotoxins, which are then internalized by receptor-mediated endocytosis [28].

In the case of BoNTs, interaction with gangliosides happens on resting motor neurons at the neuromuscular junction, which then leads to endocytosis within cycling synaptic vesicles [5]. Upon acidification of these vesicles, the catalytic domain is translocated into the cytosol, where cleavage of specific SNARE proteins is mediated by the BoNTLC[5]. These proteins play a key role in Ca^{2+}-

triggered neurotransmitter release at neuromuscular junction and their cleavage leads to the inhibition of the neurotransmitter release[5, 28]. In contrast, TeNT binds gangliosides on the cell surface of resting motor neurons and enters endosomes that transcytose into the central nervous system, where TeNT enters inhibitory neurons to block neurotransmitter release[5].

C. AIP56

Firstly identified and reported in 2005 [29], AIP56 is a key virulence factor of theGram-negative bacterium *Phdp*, a pathogen discovered and isolated during a massive perch kill that occurred in Chesapeake Bay in 1963 [30].

1. Structural features

AIP56 is produced as a precursor with a signal peptide at the N-terminal region [29]. During secretion, the signal peptide is cleaved and AIP56 becomes a 497 amino acid mature toxin, which is mainly organized into two distinct domains linked by a flexible unfolded polypeptide (linker region) and a disulfide bridge, formed by two cysteine residues - Cys^{278} and Cys^{314} (figure 2) [29, 31].

The N-terminal domain of AIP56 is highly identical to the type III effector NleC[31] and comprises a conserved zinc-binding motif, consisting of the amino acid sequence HEIVH, also present in tetanus and botulinum neurotoxins [32],that is responsible for the zinc-metalloprotease activity of AIP56 towards NF-kB (nuclear factor-kB) p65 [31]. Once it enters the host target cell cytosol, this catalytic domain cleaves p65 at the Cys39-Glu40 peptide bond, within the p65 N-terminal Rel homology domain, where several key residues for the interaction between DNA and this NF-kB subunit are located[33]. On the other hand, the C-terminal domain of AIP56, which is homologous to a hypothetical protein of *Acrythosiphonpisum* bacteriophage APSE-2[31]and to the C-terminal of a recently annotated hypothetical protein of the monarch butterfly *Danausplexippus*, plays an important role in binding and translocation of AIP56 into target cells [31].

The structural arrangement of AIP56 into two domains, one encompassing the catalytic function of the toxin and other being responsible for its transport into host target cells, led to the current classification of AIP56 as a member of the AB toxin family [34].

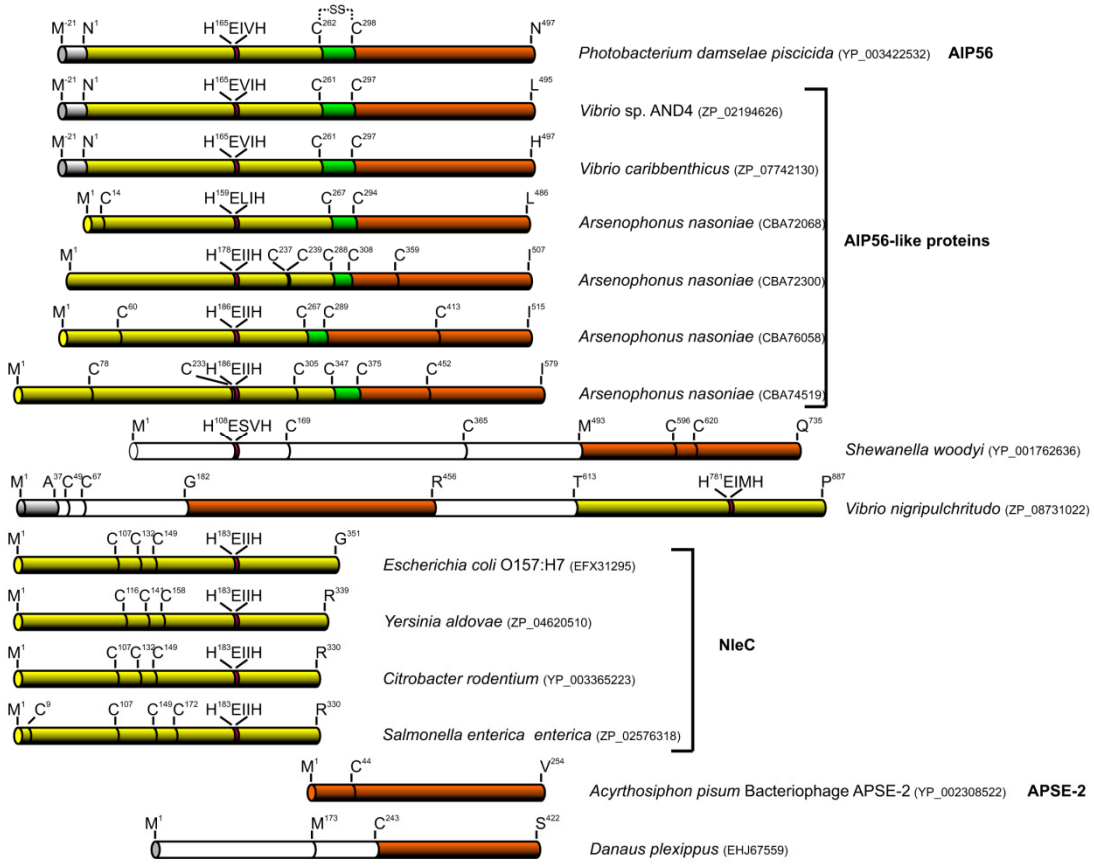

Figure 2 – Schematic diagram of the primary structure of AIP56 and AIP56-related proteins retrieved by Blast analysis. Grey: Signal peptides for AIP56 [29]and predicted for the remaining proteins; Yellow: regions with high identity to NleC and AIP56 N-terminal catalytic domain; Green: regions with high identity with AIP56 linker region; Orange: regions with high identity to APSE-2 and AIP56 C-terminal domain; Red: zinc-metalloprotease signature HEXXH; White: regions with low identity to AIP56 domains, NleC or APSE-2. Conserved zinc-metalloprotease signature HEXXH, cysteine residues, and other signalled amino acids are represented at their relative positions. (Updated from [34])

However, there are some divergent aspects between AIP56 and the other known AB toxins. For instance, bacterial AB toxins are often secreted as a single polypetide chain and undergo proteolytic nicking [8, 35], a process that is essential for toxicity, whereas in the case of AIP56, there is no evidence of proteolytic processing [31]. In addition, it has been reported that proteolytic nicking of AIP56 leads to abolishment of its toxicity [31], which opposes the role that this processing plays in the majority of AB toxins. This fact suggests that the integrity of the linker region of AIP56 is required for intoxication and points to a possible role of this region in the AIP56 translocation process [31].

Another particular feature of AIP56 relates to the role of the disulfide bond linking the A and B domains for intoxication: while the integrity of this bond is as important as nicking for the toxicity of AB toxins [36-38], in AIP56 the disruption of this bridge by alkylation only mildly decreases toxicity [31]. These facts raise interest in studying AIP56 as they show that this AB toxin evidences some uncommon features/behaviors that are not shared by the majority of toxins of the class, making it such an unique and intriguing toxin.

2. Role of AIP56 in *Phdp*pathogenesis

The contribution of AIP56 for the success of *Phdp*is quite substantial. NF-kB, and more specifically its p65 subunit, possesses anti-apoptotic properties, which are neutralized, or at least reduced, upon AIP56-mediated depletion of this transcription factor [31]. Several extrinsic and intrinsic apoptotic pathways are triggered upon intoxication by AIP56, leading to the activation of caspases -8, -9, and -3 and to the overproduction of reactive oxygen species by the mitochondria, initiated by the loss of mitochondrial membrane potential and the release of cytochrome c [36].

In acute *Phdp* infections, a rapid septicemia develops, leading to a short course of the disease and extremely high mortality rates [29, 39]. Pathologically, AIP56 contribution to the infection is based on the induction of apoptotic death of macrophages and neutrophils by the toxin, which then culminates in a secondary necrotic process with lysis of these phagocytes [40, 41]. This set of events causes the impairment of the host immune defenses as well as the release of cytotoxic contents from phagocytes, contributing to the formation of necrotic lesions that can be observed in animals affected by this disease. It has been proposed that the impairment of NF-kB transcriptional activity resulting from AIP56 activity may be the principal cause of disseminated phagocyte apoptosis observed in *Phdp* infections [29, 31].

The discovery of AIP56 and consequent disclosure of its crucial role in infection led to the establishment of this AB toxin as the main virulence factor of *Phdp* and showed a new perspective of the infection mechanism of this pathogen [29, 42]. Moreover, the identification of the toxin also led to the development of a vaccine with the purpose of impairing *Phdp*infection, one of the most threatening bacterial diseases in mariculture worldwide due to its wide host range, massive mortality, ubiquitous geographical distribution, widespread antibiotic resistance and lack of efficient vaccines [29, 34].

D. Project objectives

Although several studies were conducted in order to characterize and understand AIP56 molecular mechanism(s) of action, various aspects of its intoxication process remain undisclosed. Therefore, the main objective of this thesis was the development of molecular tools that can be used in future studies aiming at defining the exact boundaries of the region(s) involved in the AIP56 binding/translocation process.

Chapter II:

Materials and Methods

A. Constructs

The proteins used in this study were expressed in *E. coli.* The strategy used for cloning the desired DNA coding sequences into pET-28a(+) vector (Novagen) in frame with a C-terminal His-tag is described below.

1. β-lactamase moiety

The DNA sequence encoding β-lactamase amino-acids 19 to 286 (Bla^{19-286}) was cloned into pET-28a(+), using NcoI and SacI restriction sites. For this, a polymerase chain reaction (PCR) amplification was performed with primers BlaFW1NcoI/BlaRV1SacI (table 1), using plasmid p327 pBC Lgt3mut, kindly provided by Dr.Dimitri Panagiotis Papatheodorou, as template. The PCR reaction included: 1.5mM $MgCl_2$, 1x PCR buffer (Promega), 0.2 mMdeoxynucleotide triphosphates (dNTP) mix, 0.4 µM of each primer, 1 unit of GoTaq DNA Polymerase (Promega), 0.15 units of *Pfu* DNA Polymerase (Promega) and 1 µL (1:20 dilution) of template. The reaction was performed in a Thermo Scientific Piko Thermal Cycler (Thermo Scientific), with the following conditions: denaturation at 94 ºC for 2 min, 30 cycles of amplification (denaturing at 94 ºC for 45 s; annealing at 68 ºC for 30 s; extension for 72 ºC 1 min at) and final extension at 72 ºC for 5 min.

The desired fragment was excised after separation through agarose gel (1% w/v) electrophoresis, and the DNA purified using the Illustra GFX PCR DNA and Gel band purification kit (GE Healthcare), following the manufacturer's instructions.

The resulting Bla^{19-286} purified DNA was cloned in pGEM-T Easy vector (Promega), according to the technical manual. The reaction, mediated by T4 DNA Ligase, was carried out overnight at 4 ºC. Subsequently, the ligation was transformed into *E. coli* XL1 competent cells through the heat-shock method (detailed in section I.3 of this chapter). Transformants were plated on LB agar medium containing ampicillin (150 µg/mL) and isopropyl-β-D-thiogalactopyranoside (IPTG)/5-bromo-4-chloro-3-indolyl-beta-D-galacto-pyranoside (X-GAL). Positive (white) clones were inoculated in 5 mL LB medium with ampicillin (150 µg/mL) and incubated overnight at 37 ºC with with continuous shaking (200 rotations per minute (rpm)). Afterwards plasmid DNA was extracted from bacterial cultures using QIAprep® Spin Miniprep Kit (Qiagen) following the manufacturer's instructions. In order to confirm the presence of a band with the expected size (the Bla^{19-286} sequence), the minipreps were screened by restriction enzyme digestion with NcoI and SacI (Promega). Digestions were carried out in 1x Tango buffer (Fermentas), for 4 h at 37 ºC.

One positive clone was selected and the digestion performed in larger scale in order to purify an adequate amount of DNA to clone in pET28a (+). Separation, excision and purification of the desired DNA fragment were performed as described above. Finally, Bla^{19-286} purified DNA was

ligated overnight at 4 ºC to pET-28a (+) vector (previously digested with NcoI/SacI enzymes), with T4 DNA Ligase (Promega), yielding the plasmid pET28a-Bla$^{19-286}$. The ligation was used to transform *E. coli* XL1 competent cells through the heat-shock method. Transformants were plated on LB agar medium containing kanamycin (50 µg/mL) and incubated overnight at 37 ºC. Positive clones were identified by PCR using T7 and T7 terminator primers (table 1), inoculated in 5 mL LB medium with kanamycin (50 µg/mL) and incubated overnight at 37 ºC with continuous shaking (200 rpm). Afterwards plasmid DNA was extracted from bacterial cultures as previously described.

2. DTa moiety

The DNA sequence encoding the DTa region (DTa$^{26-216}$) containing the same restriction sites as the β-lactamase moiety, was similarly cloned into pET28a(+). A PCR amplification was performed using the primer set DTaFW1NcoI/DTaRV1SacI (table 1) and plasmid pET28DT, kindly provided by Dr. Dimitri Panagiotis Papatheodorou, as template. For this reaction, a mix containing 1.5 mM $MgCl_2$, 1x PCR buffer, 0.2 mMdNTP mix, 0.4 µM of each primer, 1 unit of GoTaq DNA Polymerase, 0.15 units of *Pfu* DNA Polymerase and 1 µL (1:20 dilution) of template and 0.4 µM of each primer was prepared. The PCR was performed in a Thermo Scientific Piko Thermal Cycler, with the following conditions: denaturation at 94 ºC for 2 min, 30 cycles of amplification (denaturing at 94 ºC for 45 s, annealing at 64 ºC for 30 s, extension at 72 ºC for 30 s) and a final extension at 72 ºC for 5 min. A second PCR amplification was performed under the same conditions using the PCR product from the first amplification as template. The obtained product was separated by agarose gel (1%) electrophoresis, excised and the DNA purified using Illustra GFX PCR DNA and Gel band purification kit, following the manufacturer's instructions. The purified DTa$^{26-216}$ DNA was then ligated into pGEM-T Easy vector, in a reaction mediated by T4 DNA Ligase and carried out overnight at 4 ºC. The ligation was used to transform *E. coli* XL1competent cells through heat-shock method (detailed in section I.3 of this chapter). Transformants were plated on LB agar medium containing ampicillin (150 µg/mL) and IPTG/X-GAL. Positive (white) clones were inoculated in 5 mL LB medium with ampicillin (150 µg/mL) and incubated overnight at 37 ºC with continuous shaking (200 rpm). Plasmid DNA was purified from bacterial cultures using the method described for the β-lactamase moiety. In order to confirm the presence of an insert with the expected size, minipreps were digested with restriction enzymes NcoI and SacI. These reactions were carried out in 1x Tango buffer for 2 h at 37 ºC.

One positive clone (pGEMDTa$^{26-216}$) was selected, and the restriction enzymes digestion performed in a larger scale in order to obtain an adequate amount of DNA to clone on pET28a(+). Separation, excision and purification of the desired DNA fragment were performed as previously described. Finally, DTa$^{26-216}$purified DNA was ligated overnight at 4 ºC to pET-28a(+) vector

(previously digested with NcoI/SacI enzymes), with T4 DNA Ligase, yielding the plasmid pET28a-DTa$^{26-216}$. The ligation was used to transform *E. coli* XL1 competent cells through the heat-shock method. Transformants were plated on LB agar medium containing kanamycin (50 µg/mL) and incubated overnight at 37 ºC. Positive clones were identified by PCR using T7 and T7 terminator primers (table 1), inoculated in 5 mL LB medium with kanamycin (50 µg/mL) and incubated overnight at 37 ºC with continuous shaking (200 rpm). Afterwards plasmid DNA was extracted from bacterial cultures as previously described.

3. AIP56 constructs

Three AIP56 constructs were used in this study: AIP56^{AAIVAA}, AIP56$^{210-497}$, and AIP56$^{256-497}$. They were all obtained byPCR amplification using plasmid pET28a-AIP56^{AAIVAA} (previously obtained in our lab [31]) as template, which contains the full-length catalytically inactive AIP56 mutant (AIP56^{AAIVAA}). The primer sets for each construct were as follows:

- AIP56^{AAIVAA}–AIP56FW6SacI/AIP56XhoIRV (table 1);
- AIP56$^{210-497}$ – AIP56FW7SacI/AIP56XhoIRV (table 1);
- AIP56$^{256-497}$ –AIP56FW8SacI/AIP56XhoIRV (table 1).

Of note, all constructs contain an N-terminal SacI and a C-terminal XhoI restriction sites. PCR reactions containing 1.5 mM $MgCl_2$, 1x PCR buffer, 0.2 mMdNTP mix, 0.4 µM of each primer, 1 unit of GoTaq DNA Polymerase, 0.15 units of *Pfu* DNA Polymerase and 1 µL (1:20 dilution) of template and 0.4 µM of each primer were prepared. A Thermo Scientific Piko Thermal Cycler was used, and the reaction conditions were the following: denaturation at 94ºC for 2 min, 30 cycles of amplification (denaturing at 94 ºC for 45 s; annealing at 68 ºC for 30 s; extension at 72 ºC for 1 min) and a final extension at 72 ºC for 5 min. Afterwards, the PCR products were separated in agarose gels (1%), and the desired DNA fragments purified from excised bands using Illustra GFX PCR DNA and Gel band purification kit. The resulting purified DNAs were then ligated into pGEM-T Easy vector (Promega) under the same conditions used for the reporter moieties. Each ligation was used to transform *E. coli* XL1 competent cells through heat-shock method (detailed in section I.3 of this chapter). Transformants were plated on LB agar medium containing ampicillin(150 µg/mL) and IPTG/X-GAL. Positive (white) clones were inoculated in 5 mL LB medium with ampicillin (150 µg/mL) and incubated overnight at 37 ºC with continuous shaking (200 rpm).Afterwards plasmid DNA of each construct was purified from bacterial cultures as previously described. In order to confirm the presence of the inserts with the expected size, minipreps were digested with restriction enzymes SacI and XhoI. These reactions were carried out in 1x Tango buffer for 2 h at 37 ºC.

One positive miniprep clone from each construct (pGEMAIP56^{AAIVAA}, pGEMAIP56$^{210-497}$ and pGEMAIP56$^{256-497}$) was selected, and the restriction enzymes digestions performed in larger scale

in order to obtain an adequate amount of DNA to clone in pET28a-Bla$^{19-286}$or pGEMDTa$^{26-216}$. The pGEMAIP56^{AAIVAA}reaction was performed in 1x Tango buffer (Fermentas) during 2 h at 37ºC, while both pGEMAIP56$^{210-497}$ and pGEMAIP56$^{256-497}$ reactions were carried out in 1x BamHI buffer (Promega) overnight at 37 ºC. Separation, excision and purification of the desired DNA fragment were performed as previously described.

Finally, all AIP56 constructs were cloned into pETDTa$^{26-216}$ and pETBla$^{19-286}$, previously linearized with SacI/XhoI enzymes, using T4 DNA Ligase during a 2 days reaction at 4 ºC. The ligation was used to transform *E. coli* XL1 competent cells through the heat-shock method. Transformants were plated on LB agar medium containing kanamycin (50 µg/mL) and incubated overnight at 37 ºC. Positive clones were identified by PCR using T7 and T7 terminator primers (table 1), inoculated in 5 mL LB medium with kanamycin (50 µg/mL) and incubated overnight at 37 ºC with continuous shaking (200 rpm). Afterwards plasmid DNA was extracted from bacterial cultures as previously described.In order to ensure the absence of sequence errors, and the presence of C-terminal His-tags, one positive miniprep clone from each construct (table 2; figure 3) was selected and sequenced with vector primers T7 and T7 terminator and other specific primers detailed in table 1. All samples were sequenced at MWG (http://www.mwg-biotech.com) or GATC (http://www.gatc-biotech.com).

Table 1 – Primers used in thiswork

Primer Designation	Nucleotide Sequence	Purpose
BLAFW1NCOI	5' - GGGCCATGGGGCTTCCTGTTTTTGCTCACCCAGAA - 3'	For design of constructs A1, B1, C1
BLARV1SACI	5' - CCCGAGCTCCCAATGCTTAATCAGTGAGGC - 3'	For design of constructs A1, B1, C1
AIP56FW6SACI	5' – CCGGAGCTCAACAACGATAAACCAGATGC – 3'	For design and sequencing of constructs A1, A2
AIP56FW7SACI	5' – CCCGAGCTCCCTGCGAGGGTCGAAGCG – 3'	For design of constructs B1, B2
AIP56FW8SACI	5' – CCGGAGCTCACCTCTTTTTGCTCGGAAGG – 3'	For design of constructs C1, C2
AIP56 XHOI RV	5' – ACGCGCCACAATTCATTAATCTCGAGCGC – 3'	For design of constructs A1, A2, B1, B2, C1, C2
DTAFW1NCOI	5' – CCCCCATGGGGATGGCTAGCATGGGC - 3'	For design of constructs A2, B2, C2
DTARV1SACI	5' - CCCGAGCTCGACACGATTTCCTGCAC – 3'	For design of constructs A2, B2, C2
T7	5' – TAATACGACTCACTATAGGG – 3'	For positive clone selection by PCR and sequencing of all constructs
T7 terminator	5' - GCTAGTTATTGCTCAGCGG – 3'	For positive clone selection by PCR and sequencing of all constructs

Table 2 – Constructs produced in this work

Construct	Designation
$Bla^{19-286}AIP56^{AAIVAA}$	A1
$DTa^{26-216}AIP56^{AAIVAA}$	A2
$Bla^{19-286}AIP56^{210-497}$	B1
$DTa^{26-216}AIP56^{210-497}$	B2
$Bla^{19-286}AIP56^{256-497}$	C1
$DTa^{26-216}AIP56^{256-497}$	C2

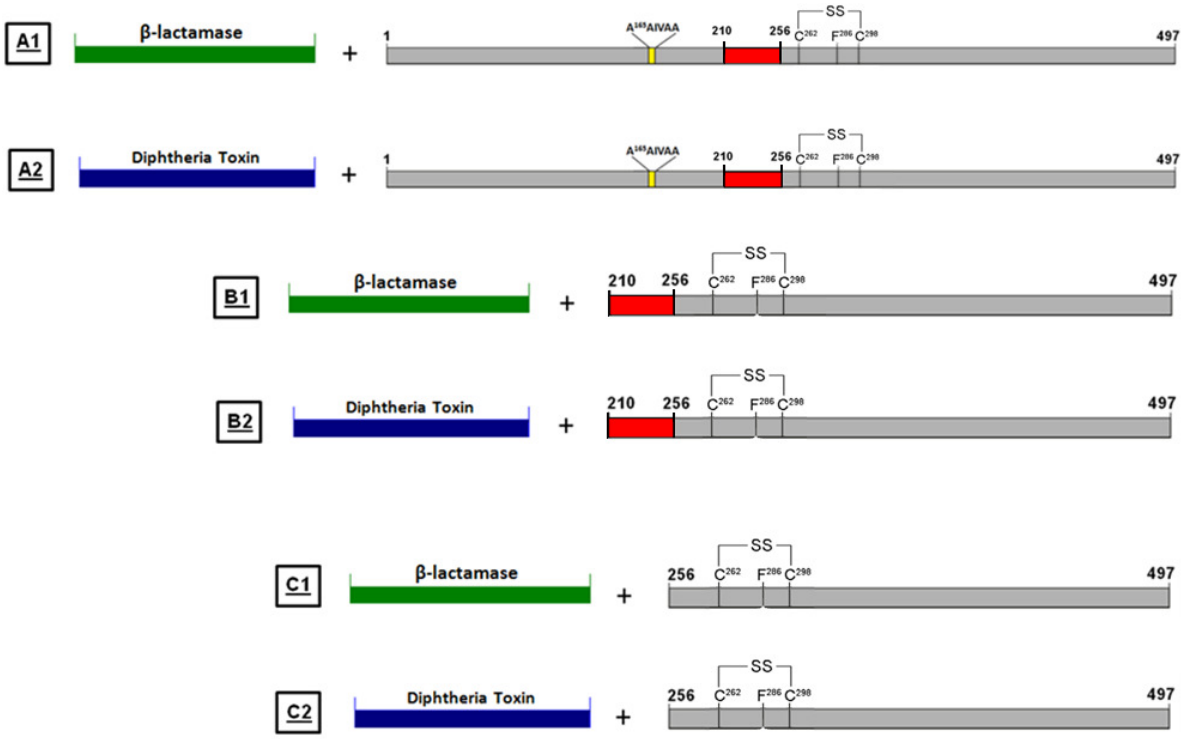

Figure 3 – Representativescheme of all constructs designed in this work. Sequences corresponding to Bla^{19-286} (green), DTa^{26-216} (blue), AIP56 (gray) and the AIP56 region encompassing the T1-like motif and the two helices upstream of this motif (red) are shown.

B. Protein production

After construct integrity verification by sequencing (not shown), the six constructs (Table 2) in pET28a were transformed in the *E. coli* expression strain BL21 (DE3) (please see section K.3 for a

detailed description). Selected clones from each construct in BL21(DE3) were inoculated in 5 mL LB supplemented with 50 µg/mL kanamycin and incubated overnight at 37 ºC with continuous shaking (200 rpm). The initial cultures were diluted 1:100 in 400 mL of fresh LB with 50 µg/mL kanamycin and incubated at 37 ºC with continuous shaking (200 rpm), until the OD_{600nm} reached 0.4. Then, the cultures were transferred to 17 ºC and incubated with continuous shaking (165 rpm) until an OD_{600nm} of 0.6 was reached. In order to induce protein expression, IPTG was added to a final concentration of 1 mM, and the cultures kept at 17 ºC with continuous shaking (165 rpm) for 4h. Induced cultures were collected and centrifuged for 30 min at 4000 g, 4 ºC. Pellets were resuspended in lysis buffer (50 mMsodium phosphate buffer pH 7.4, 500 mMNaCl, 200 µg/mL lysozyme, 100 µg/mL PMSF and 10% glycerol) in a ratio of 1.75 mL buffer per 50 mL culture. DNAse I (Sigma) and $MgCl_2$ were added to final concentrations of 10 µg/mL and 10 mM, respectively. After 30 min incubation on ice, samples were sonicated on ice (4x 10 s with 20 s intervals) with a Sonifier B-12 (Branson). Soluble and insoluble fractions were separated by a centrifugation step at 21000 g, 4 ºC for 20 min. Samples of total lysates, soluble and insoluble fractions were collected and stored at - 20 ºC for further analysis.

C. Protein purification

His-tagged AIP56 chimeras were purified from the soluble fractions of induced bacterial cells by affinity chromatography using the HisTrap™ HP 1 mL (GE Healthcare). Initially, these soluble fractions were supplemented with 15 mM Imidazole, filtered with a 0.2 µm filter (Frilabo) and loaded onto the chromatography column. Successfully bound proteins were eluted, at a flow rate of 1 mL/min, with step-increasing concentrations of imidazole in 50 mM sodium phosphate buffer pH 7.4, 500 mMNaCl, 10% glycerol. To the fractions containing the desired protein an equivalent volume of 50 mM sodium phosphate buffer pH 7.4, 500 mMNaCl was added in order to lower protein and imidazole concentrations and minimize AIP56 precipitation. These fractions were pooled and buffer exchanged to 20 mMTris-HCl pH 8.0, 200 mMNaCl, 5% glycerol using a PD10 desalting column (GE Healthcare), according to the gravity protocol provided by the column's manufacturer. Samples were concentrated using Amicon ® Ultracel 50 k centrifugal filter, or Amicon®Ultracel 10 k centrifugal filter in the case of protein C2. Fusion proteins were stored at - 20 ºC until further analysis and their concentration was determined by 280 nm absorbance measurement using Nanodrop 1000 (Thermo Scientific).

D. Crude β-lactamase extract preparation

Preparation of crude β-lactamase extract, used in β-lactamase *in vitro* activity assay, was

performed following the protocol described in [43]. Briefly, *E. coli*BL21(DE3) competent cells were transformed with plasmid pET-23b(+) (Novagen), which already contains the gene encoding β-lactamase, using the heat-shock method. Transformants were inoculated in 5 mL LB supplemented with 150 µg/mL ampicillin and incubated overnight at 37 ºC with continuous shaking (165 rpm). This culture was then diluted 1:100 in fresh LB with 150 µg/mL ampicillin and incubated at 37 ºC, with continuous shaking (165 rpm), until the OD_{600nm} reached 1.0. Afterwards bacterial cultures were collected and centrifuged twice for 30 min at 4000 g (4ºC). In each time, the pellet was resuspended with 100 mM sodium phosphate buffer pH 7.0 in a ratio of 1.75 mL buffer per 50 mL culture. DNase I and $MgCl_2$ were added to final concentrations of 10 µg/mL and 10 mM, respectively. Samples were incubated on ice for 30 min and then sonicated on ice (4x 15 s with 30 s intervals) with a Sonifier B-12. Finally, lysates were centrifuged for 20 min at 21000g (4ºC) and supernatant was collected, stored at -20 ºC, and later used as the crude enzyme for the β-lactamase enzymatic assay.

E. Activity of the β-lactamase-AIP56 chimeras -*in vitro* assay

Evaluation of β-lactamase activity in chimeras A1, B1 and C1 was carried out by enzymatic kinetic assay using nitrocefin (Calbiochem), a specific substrate for β-lactamase. For this method, a 96-Well Polystyrene Round Bottom Microwell Plate (Nunc®) was used and the following 100 µL mixtures prepared (in duplicate):

Table 3 – Reaction mixtures prepared for *in vitro*β-lactamase-AIP56 activity assay

Condition Additives	Blank	Positive control	Negative control	Fusion protein A1	Fusion protein B1	Fusion protein C1
Sodium phosphate buffer pH 7.0 (100 mM)	90 µL	82 µL	90 µL	82 µL	82 µL	82 µL
DMSO	10 µL	-	-	-	-	-
Nitrocefin (0.4 mM; in DMSO)	-	10 µL	10 µL	10 µL	10 µL	10 µL
Crude β-lactamaseextract	-	8 µL	-	-	-	-
Purified fusion protein A1 (168 µM)	-	-	-	8 µL	-	-
Purified fusion protein B1 (46 µM)	-	-	-	-	8 µL	-
Purified fusion protein C1 (153 µM)	-	-	-	-	-	8 µL
Final volume	100 µL	100 µL	100 µL	100 µL	100 µL	100 µL

The 96-well plate was mixed for 15 s and incubated for 1 h at 30 ºC in Synergy 2 SL Luminescence Microplate Reader (Bio-Tek). During the incubation, the microplate was read every minute at 390 nm and 486 nm.

F. Activity of the DTa-AIP56 chimeras - *in vitro* assay

The activity of DTa in chimeras A2, B2 and C2 was tested by evaluation of protein synthesis inhibition using an *in vitro* assay. For that, a ^{35}S-labeled protein production in rabbit reticulocyte lysates by *in vitro* translation using the TNT T7 Quick Coupled transcription/Translation kit (Promega) was performed following the manufacturer's instructions but in the presence of different conditions, including the chimeric proteins. Five microliters of rabbit reticulocyte lysates supplemented with 1 µg/µL NAD^+ (Sigma) were pre-incubated for 10 min at 30 ºC in the presence of the additives described in table 4:

Table 4 – Additives used for *in vitro* DTa-AIP56 activity assay

Conditionnr.	Additive	Stockconcentration	Dilution	Volume added (µL)
1	AIP56	56 µM	1:10	0.1
2	DT	25µM	1:100	0.25
3	Fusion protein B2	18 µM	-	0.25
4	Fusion protein B2	18 µM	1:10	0.25
5	Fusion protein C2	167 µM	1:10	0.3
6	Fusion protein C2	167 µM	1:100	0.3
7	Fusion protein A2	10 µM	-	0.32
8	Fusion protein A2	10 µM	1:10	0.32
9	Fusion protein A1	168 µM	1:20	0.36
10	Fusion protein A1	168 µM	1:200	0.36
11	Ciclohexamide	20mM	-	0.3
12	None	-	-	-
13	None (Lysate only - without NAD^+)	-	-	-

Afterwards, 1µL sbp65Rel DNA in pET28a(+) (54 ng/µL) [31] and 0.25 µL [^{35}S] methionine (11µCi/mL; PerkinElmer) were added to each condition and mixtures were incubated for 90 min at 30 ºC. The reaction was stopped on ice and a 0.5 µL sample from each reaction was mixed with 20 µL Gel Loading Buffer and boiled at 95 ºC for 5 min. The proteins were resolved in a 14% polyacrilamide gel with 1% (w/v) SDS as described in section I.4 of this chapter. After SDS-PAGE,

proteins were transferred onto a nitrocellulose membrane in a Trans-Blot SD Semi-Dry Electrophoretic Transfer Cell (Bio Rad) with an applied current of 19 V for 1h. The membrane was stained with Ponceau-S and air dried. Finally, an X-ray film was exposed directly to the membrane for 48 h and the presence of ^{35}S-labeled protein assessed by autoradiography.

G. Primary cultures of mouse bone marrow derived macrophages (mBMDM)

mBMDM cells were derived from bone marrow progenitors extracted from the femurs of 1-3 month-old C57BL/6 male mice. In order to collect the bone marrow, each femur was flushed with 5 mL of ice cold HBSS (Hank's balanced salt solution; ref. 14060040; Invitrogen). The collected cell suspension was centrifuged for 10 min at 285 g (4 ºC) and the pellet resuspended in 4 mL DMEM (Dulbecco's modified essential medium; ref. 10938; GIBCO) supplemented with 10% fetal bovine serum (FBS; Life Technologies), 10 mM glutamine, 10 mM HEPES, and 1 mM sodium pyruvate (hereafter designated complete DMEM). To separate fibroblasts from the desired cells, the cell suspension was transferred to a cell culture dish, to which 12 mL complete DMEM and 10% L929 cell-conditioned media (LCCM) had been previously added, and the plate incubated overnight at 37 ºC with 7% CO_2 in a humidified incubator. Then, non-adherent cells were collected and the plate washed 3x with 10 mL ice cold HBSS. The cell suspension was centrifuged 10 min at 285 g (4 ºC) and the pellet resuspended in 4 mL of complete DMEM. For counting, cells were diluted 1:10 in trypan blue dye and a Neuebauer chamber was used. After adjusting the cell concentration to $5x10^5$ cells/mL by addition of complete DMEM with 10% LCCM, 1 mL cell suspension ($5x10^5$ cells) or 0.2 mL ($1x10^5$ cells) were distributed per well in 24-well plates or 96-well plates, respectively. At day 4, 10% of LCCM was added per well and at day 7 the cell medium was refreshed. Since collection, cells were kept at 37ºC with 7% CO_2 in a humidified incubator; they were used at day 10, when macrophages reached full differentiation.

H. Substrate loading optimization for *in vivo* assays of β-lactamase-AIP56 chimeras

For future *in vivo* assays of β-lactamase-AIP56 chimeras A1, B1 and C1 using CCF4-AM substrate provided with the LiveBLAzer^{TM} FRET – B/G Loading Kit (K1095; Invitrogen), a screening for optimal conditions of substrate loading was performed. For this purpose, mBMDMs in 96-well plates (prepared as described in section G of this chapter), were loaded with the recommended amount of standard substrate loading solution (prepared according to the manufacturer's instructions) and incubated at room temperature (RT), in the dark, for periods of 30 min to 4 h.

Substrate loading was evaluated, at different time points, by microscopy, using aninverted epifluorescence microscope (Leica DMI 6000B).

I. *In vivo* assay of β-lactamase-AIP56 chimeras

The ability of the β-lactamase-containing chimeras to translocate this reporter moiety to the cytosol of mBMDM was evaluated using the previously optimized conditions of substrate loading (section H). Firstly, mBMDM in 96-well plates were pre-incubated with chimeras A1, B1 or C1 for 1 h at 37ºC with 7% CO_2 in a humidified incubator. In parallel, mBMDM were incubated in the same conditions with LFnBla (2 µg/mL) + PA (1µg/mL) mixture ([46]; both kindly provided by Dr. Stephen Lepla) or without any chimera, corresponding to the positive and negative control conditions, respectively. Afterwards, the cells were washed with 1x phosphate buffered saline (PBS; 137 mM NaCl, 2.7 mM KCl, 10 mMNa_2HPO_4, 2 mM KH_2HPO_4) and loaded with the recommended amount of standard substrate loading solution (prepared according to the manufacturer's instructions) and incubated at room temperature (RT), in the dark, for 30 min. Substrate cleavage and FRET disruption was then evaluated by microscopy, using an inverted epifluorescence microscope (LeicaDMI 6000B). The excitation wavelength used was 409 nm and the fluorescence emission was tracked at 520 nm (corresponding to the intact substrate) and 450 nm (corresponding to the cleaved substrate). The results were analyzed using one-way anova.

J. *In vivo* assay of DTa-AIP56 chimeras

DTa-AIP56 chimeras translocation to the cytosol was tested using mBMDM. Cells were pre-incubated for 1 h at37ºC, 7% CO_2 in a humidified incubator in RPMI 1640 medium without methionine (Sigma, R7513), supplemented with 10% FBS, 1% P/S, 10 mM HEPES, 1 mM piruvate, 10 mM L-glutamine, 1% non-essential aminoacids and 10% LCCM. Afterwards the medium was replaced with fresh medium containing either the testing chimeras (100 nM), AIP56 (178 nM), AIP56Mut ($AIP56^{AAIVAA}$; 178 nM) or the positive controls DT (10 nM) or cicloheximide (500 µM) and the cells were incubated for 16 h at 37ºC, 7% CO_2 in a humidified incubator. Next, the medium was replaced by fresh medium containing 1 µCi [^{35}S] Methionine followed by 1 h incubation at 37ºC, 7% CO_2 in a humidified incubator. The medium was removed, 5% TCA was added to each well and the plate was centrifuged at 4000 g for 10 min (4ºC). Next, the supernatant was discarded, the monolayer was washed 3x with 70% ethanol and lysed with 0.1 M NaOH + 0.1 % SDS. Samples were transferred to 1.5 mL tubes, 300 µL liquid scintillation cocktail (MP

Biomedicals; ref: 01882480) was added to each sample and the radioactive aminoacid incorporation was measured using 1450 LSC &Luminescence counter (PerkinElme – MicrobetaTrilux).

K. Miscellaneous

1. Agarose gel electrophoresis

Before electrophoresis, DNA samples were stained with loading buffer 5x (Bioline), loaded into a 1% agarose gel containing 1x RedSafe (iNtRON) and run at 120 volts (V). Afterwards, gel was imaged using Gel Doc XR System (Bio-Rad) and DNA samples quantified using ImageLab software.

2. Sequence analysis

Protein sequence alignments were performed using ClustalW2 multiple sequence alignment tool (http://www.ebi.ac.uk/Tools/msa/clustalw2/). Theoretical molecular weights and isoelectric points were calculated using the ProtParam tool (http://web.expasy.org/protparam/).

3. Bacterial transformation (heat-shock method)

All transformations performed in this study were carried out accordingly to the heat-shock method. Furthermore, 100 µL aliquots of *E. coli* XL1 Blue or BL21 (DE3) competent cells were always used to transform the prepared ligations (vector plus DNA of interest). Briefly, competent cells were thawed on ice for 10 minutes. Secondly, they were incubated for 30 min on ice with the ligations, heat-shocked for 90 s at 42 ºC and immediately incubated for 2 min on ice for recovery. Next, 4 volumes of Super Optimal broth medium with Catabolite repression (SOC) medium (2% Tryptone, 1% Yeast Extract, 10 mM NaCl, 2.5 mM KCl, 10 mM $MgCl_2$, 10 mM $MgSO_4$ and 20 mM Glucose) were added to the volume of bacteria and the suspension incubated, at 37 ºC for 45-60 min with continuous shaking (200 rpm). Finally, transformants were plated on LB agar medium containing the appropriate antibiotic (50 µg/mL kanamycin for pET-28a(+) plasmids, 100 µg/mL chloramphenicol for p327 plasmid and 150 µg/mL ampicillin for pGEM-T Easy and pET-23b(+) plasmids) and incubated overnight at 37 ºC.

4. SDS-PAGE

Reducing sodium dodecyl sulfate - polyacrylamide gel electrophoresis (SDS-PAGE) was

performed using the Laemmli discontinuous buffer system [44]. For SDS-PAGE analysis, samples were boiled for 5 min at 95 ºC in gel loading buffer (GLB; 50 mMTris-HCl, pH 8.8, 2% SDS, 10% glycerol, 0.017% bromophenol blue, 2 mM EDTA (Ethylenediaminetetraacetic acid) pH 8.8, 100 mM DTT (Ditiotreitol)) and proteins were resolved in 12% or 14% polyacrilamyde gels with 1% (w/v) SDS. After electrophoresis, gels were either stained with Coomassie Blue R-250 (Sigma Chemical) or transferred onto nitrocellulose membranes.

5. Western Blotting

After SDS-PAGE, proteins were transferred onto nitrocellulose membrane in a Trans-Blot SD Semi-Dry Electrophoretic Transfer Cell with an applied current of 19 Vfor 1h. Nitrocellulose membranes were stained with Ponceau S and washed with distilled water.

For histidine tag (His-tag) detection, the following protocol was applied: membrane blocking was performed using 5 % low fat milk in tris-buffered saline (TBS; 50 mM Tris-HCl, pH 7.5; 150 mM NaCl) containing 0.1% Tween 20 (T-TBS) for 1h at RT. The membrane was incubated with anti-His-tag primary antibody (1:1000 in 5 % low fat milk in T-TBS) overnight at 4 ºC. Membrane was washed 3x (5 min each wash) with T-TBS at RT, incubated with anti-mouse alkaline phosphatase conjugate (1:10 000 in 5 % low fat milk in T-TBS) for 1 h at RT, and washed with T-TBS as previously described. Reactive bands were detected by BCIP/NBT development. The reaction was stopped with distilled water.

For AIP56 detection, the following protocol was performed: membrane blocking was performed ON at 4 ºC using 5 % low fat milk in T-TBS (0.1 % Tween 20). Membrane was incubated with anti-AIP56 MT1415 2ndbleed primary antibody (1:5000 in 5 % low fat milk in T-TBS) for 1 hat RT and washed 3x (5 min each wash) with T-TBS. Incubation with anti-rabbit alkaline phosphatase conjugate (1:30 000 in 5 % low fat milk in T-TBS) was performed at RT for 1 h, and membrane was washed as previously described. Reactive bands were detected by BCIP/NBT development. The reaction was stopped with distilled water.

Chapter III:

Results and discussion

In recent studies aiming at understanding the role of the two identified AIP56 structural domains [31], it was shown that the C-terminal domain does not exhibit proteolytic activity towards p65 *in vivo* or *in vitro*. However, the C-terminal region efficiently prevents AIP56 toxic effects when used as a competitor, which demonstrates its involvement in the toxin binding/internalization [31]. Furthermore, the role of the exposed flexible linker region was also studied. It was reported that chymotrypsin nicking of AIP56 at this region abolished the toxicity of AIP56 for cells, but did not affect its proteolytic activity *in vitro* [31]. Based on these observations, the authors proposed that the AIP56 linker region is required to the binding/internalization process and may even be part of the translocation domain [31]. Even though several regions that contribute for the AIP56 binding/internalization mechanism were identified, the exact boundaries of the domain responsible for these processes were not yet established.

Therefore, in order to identify the AIP56 binding/internalization domain, six chimeric proteins, consisting in different AIP56 C-terminal truncates fused with two distinct reporter moieties were designed, produced and purified.

One of the reporters used is β-lactamase, a 29-kDa enzyme that cleaves β-lactam-containing molecules like penicillins and cephalosporins [45]. Some of its commercial substrates, such as CCF2 or CCF4, possess two fluorophores (7-hydroxycoumarin and fluorescein in the case of CCF4) that exhibit efficient FRET(fluorescence resonance energy transfer). In CCF4 substrate, excitation of coumarin (at 409 nm) results in FRET to the fluorescein, which emits a green fluorescence signal (at 520 nm). In the presence of β-lactamase, FRET is disrupted by cleavage of the cephalosporin that links the two fluorophores, leading to a shift on the substrate emission wavelength (450 nm for coumarin) that can be tracked by fluorescence detection (LiveBLAzer™ FRET – B/G Loading Kit (K1095; Invitrogen)) [45]. Due to its sensitivity, robustness and ease-of-use, among other advantages, β-lactamase is a very useful reporter system [45]. Moreover this enzyme has already been used as a reporter moiety in the study of anthrax toxin uptake in various cell types through fusion with the lethal factor of this toxin [46]. In this study, the authors were able to show that macrophages, dendritic cells and B cells appear to be more sensitive than T cells to anthrax LF through the use of a β-lactamase containing chimera.

Despite the β-lactamase advantageous features, it was not known if this enzyme possessed the required properties for cell internalization and translocation mediated by AIP56. Unpublished data from our laboratory show that, similarly to other AB toxins that reach the eukaryotic cell cytosol by translocating from endossomes, translocation of AIP56 catalytic domain is triggered by endossomal acidification. It has been shown that AIP56 undergoes pH-driven structural rearrangements when exposed to acidic pH and it is likely that these structural changes are required for translocation to occur. Therefore, the use of β-lactamase as the reporter moiety may be jeopardized if this enzyme does not possess the proper mechanism of unfolding/refolding

required for AIP56-mediated translocation. Furthermore, due to the fact that the dimensions and the type of pore formed by AIP56 on the endossomal membrane are yet to be unveiled, there was no certainty that β-lactamase has the right size/conformation to undergo translocation through this structure.

Therefore, an alternative reporter moiety was used: the DTa domain. In addition to being a member of the AB family, DT also possesses an easy enzymatic readout and its catalytic domain has been previously used as a reporter moiety in other studies [47]. For instance, DTa domain was used in the study of *Pasteurella multocida* toxin as a potential transporter of non-cell-permeating proteins [47].

The definition of AIP56 truncates boundaries was based on previous reports of a conserved 10 amino acid motif, designated T1, common to DT, anthrax lethal factor, anthrax edema factor and BoNT serotypes A, C and D (reviewed in [8]). In each instance, the motif is located in a region of the toxin that emerges through the vesicle pore into the cytosol in the initial steps of translocation [8]. Therefore, an AIP56 C-terminal truncate containing the T1-like motif (located prior to the linker region) and a region upstream of this motif comprised of a predicted helix and a amphipathic helix was designed (truncate B). In order to evaluate if the region described above plays an important role in AIP56 translocation mechanism, a second truncate was designed comprising the C-terminal domain and the region downstream the T1-like motif. A full-length AIP56 mutant, whose zinc-binding motif HEIVH was mutated to AAIVA resulting in the inactivation of the AIP56 catalytic activity of AIP56 was used as a control.

Constructs coding for all chimeric proteins were obtained by standard cloning techniques. All sequences were cloned between the NcoI/XhoI restriction sites of pET-28a(+) vector in frame with a C-terminal 6xHis-tag, for later purification. The resulting construct sequences were confirmed by sequencing.

A. Optimization of expression conditions

The first AIP56 construct (designated as construct A1(see figure 3 – chapter II) consisted of the full-length AIP56 mutant, encompassing amino-acids 1 to 497, fused with a β-lactamase moiety comprising amino-acids 19 to 286, as previously used in other studies [43]. Construct A2 was designed using the same strategy applied for chimera A1; however, in this case, the reporter moiety used was DTa, which corresponds to amino-acids 26 to 216 of DT. Both A1 and A2 were used as controls for the functional experiments. Constructs B1 and B2, comprised an AIP56 C-terminal truncate, containing amino-acids 210 to 497 fused with β-lactamase and DTa, respectively. Finally, C1 and C2 constructs encompassed a shorter AIP56 C-terminal truncate, containing amino-acids 256 to 497 fused with, respectively, β-lactamase and DTa moieties.

Fusion proteins were expressed in *E. coli* using, as first approach, the production protocol

previously used for wild type AIP56 [29]. However, due to a low yield of soluble protein, a kinetic test was performed in order to evaluate the protein expression profile. In this test, the variable condition was the incubation time after induction with IPTG. For all proteins tested, the highest ratio soluble protein/L culture was obtained with a 4 h induction at 17 ºC (figures4-7).

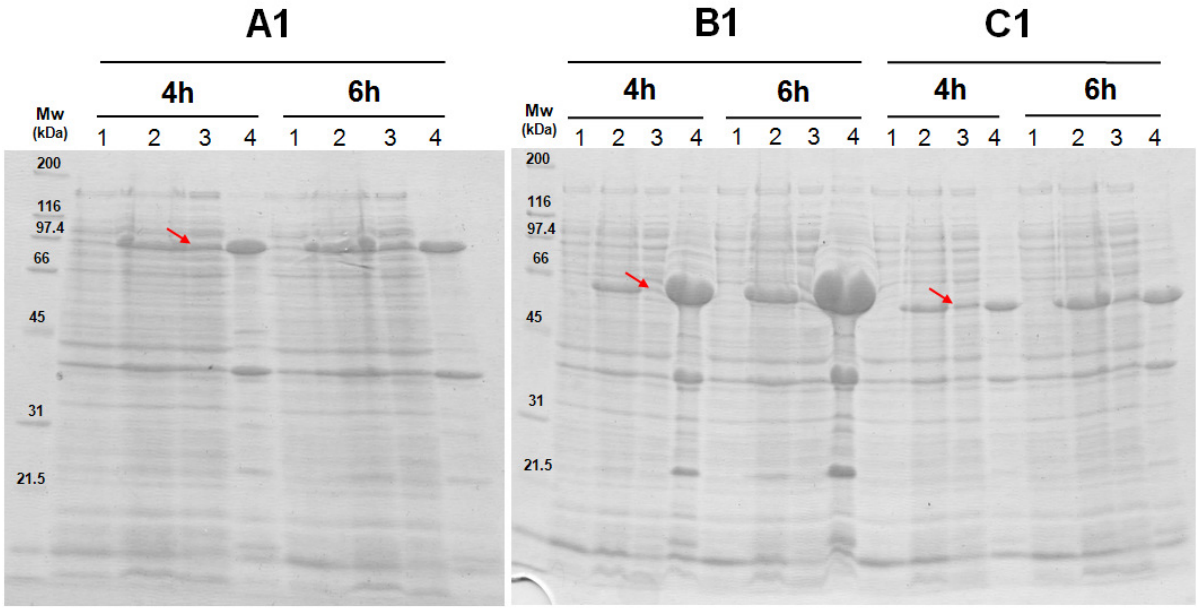

Figure 4 – Kinetics of expression of chimeras A1, B1 and C1 in *E. coli* BL21(DE3) at 17 ºC. In this test, recombinant protein expression was induced with 1 mM IPTG and the variable condition was the incubation time after addition of IPTG. Each lane contains the equivalent to 200 µL bacterial culture. Non-induced (lane 1), induced (lane 2), soluble (lane 3) and insoluble (lane 4) fractions were collected and analyzed by SDS-PAGE. Proteins in the gels were stained with Coomassie-blue. Expression profiles of chimera A1, B1 and C1 after 4 h and 6 h inductions are shown. The red arrows indicate the fusion protein bands in the soluble fractions obtained after 4 h induction with IPTG.

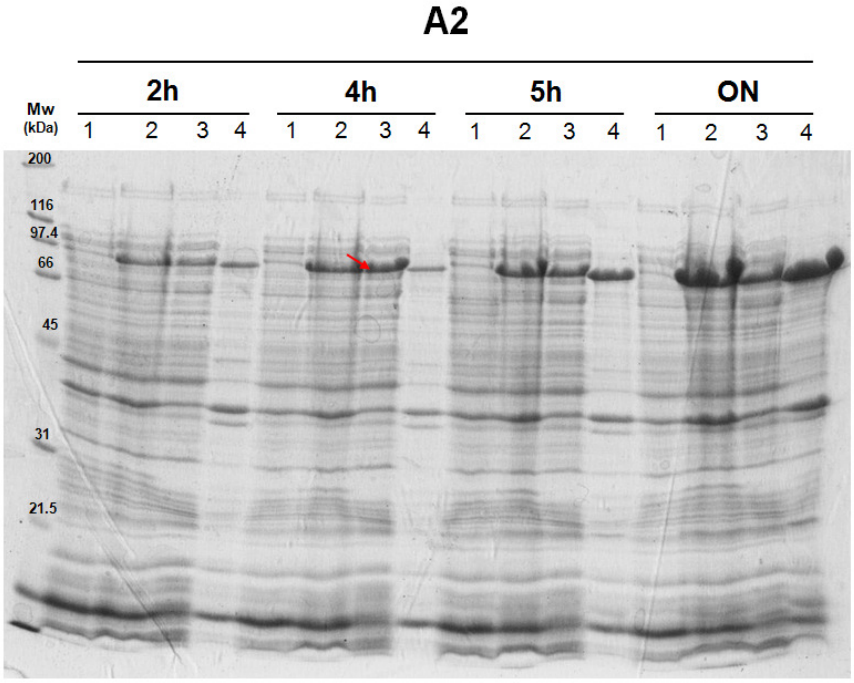

Figure 5 – Kinetics of expression of chimeras A2 in *E. coli* BL21(DE3) at 17 ºC. In this test, recombinant protein expression was

induced with 1 mM IPTG and the variable condition was the incubation time after addition of IPTG. Each lane contains the equivalent to 200 µL bacterial culture. Non-induced (lane 1), induced (lane 2), soluble (lane 3) and insoluble (lane 4) fractions were collected and analyzed by SDS-PAGE. Proteins in the gels were stained with Coomassie-blue. Expression profiles of chimera A2 after 2 h, 4 h, 5 h and overnight (ON) inductions are shown. The red arrows indicate the fusion protein bands in the soluble fractions obtained after 4 h induction with IPTG.

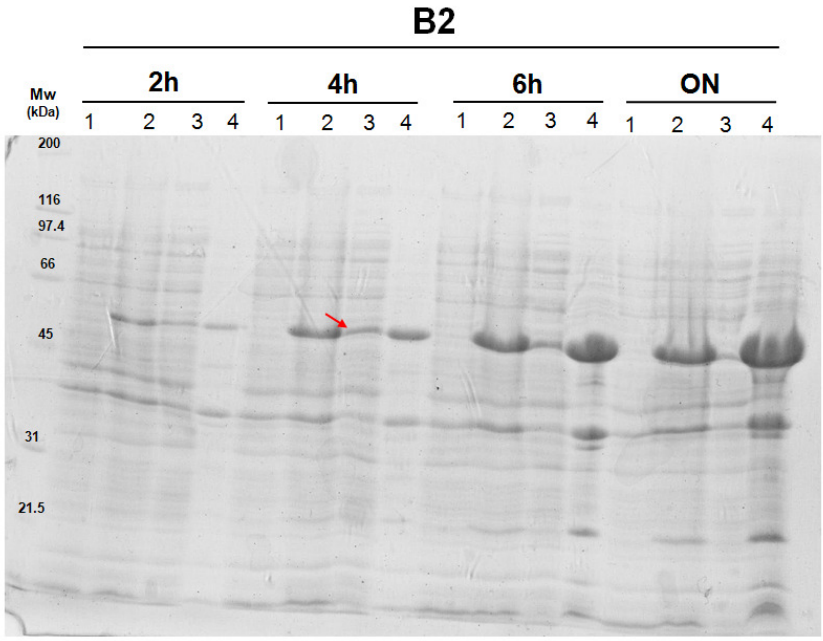

Figure 6 – Kinetics of expression of chimeras B2 in *E. coli* BL21(DE3) at 17 ºC. In this test, recombinant protein expression was induced with 1 mM IPTG and the variable condition was the incubation time after addition of IPTG. Each lane contains the equivalent to 200 µL bacterial culture. Non-induced (lane 1), induced (lane 2), soluble (lane 3) and insoluble (lane 4) fractions were collected and analyzed by SDS-PAGE. Proteins in the gels were stained with Coomassie-blue. Expression profiles of chimera B2 after 2 h, 4 h, 6 h and overnight (ON) inductions are shown. The red arrows indicate the fusion protein bands in the soluble fractions obtained after 4 h induction with IPTG.

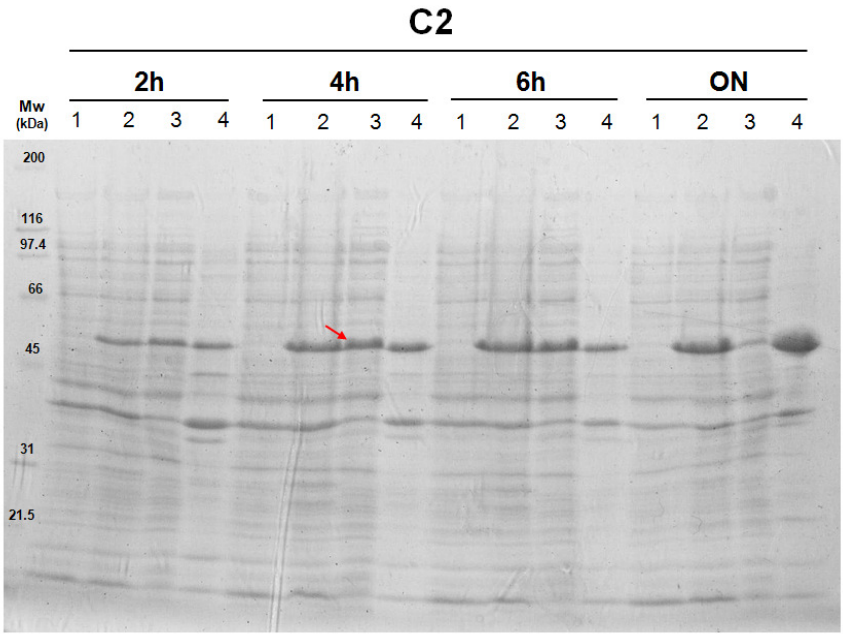

Figure 7 – Kinetics of expression of chimeras C2 in *E. coli* BL21(DE3) at 17 ºC. In this test, recombinant protein expression was

induced with 1 mM IPTG and the variable condition was the incubation time after addition of IPTG. Each lane contains the equivalent to 200 µL bacterial culture. Non-induced (lane 1), induced (lane 2), soluble (lane 3) and insoluble (lane 4) fractions were collected and analyzed by SDS-PAGE. Proteins in the gels were stained with Coomassie-blue. Expression profiles of chimera C2 after 2 h, 4 h, 6 h and overnight (ON) inductions are shown. The red arrows indicate the fusion protein bands in the soluble fractions obtained after 4 h induction with IPTG.

B. Protein purification

After expression, induced soluble fractions were subjected to nickel-affinity chromatography. First, trial-scale purifications (batch procedure) under native conditions using nickel affinity resin were performed. However, an extremely low yield was obtained (data not shown). In order to surpass this problem, denaturing (using urea as denaturing agent) and reducing (using DTT as reducing agent) conditions were tested for the same protocol. In all conditions, the yield was very low (data not shown). This resulted from an inefficient binding of the recombinant proteins to the resin, as almost all protein was retained in the non-ligated fraction (data not shown). To investigate if the low binding could result from the absence of the His-tag in the fusion proteins, these were subjected to a Western Blotting using anti-HIStag antibody (figure 8) which confirmed the presence of the tag in all recombinant proteins, in accordance to the sequencing results of the constructs. Furthermore, as expected, all fusion proteins were also recognized by an anti-AIP56 antibody, used as a positive control for Western Blotting procedure.

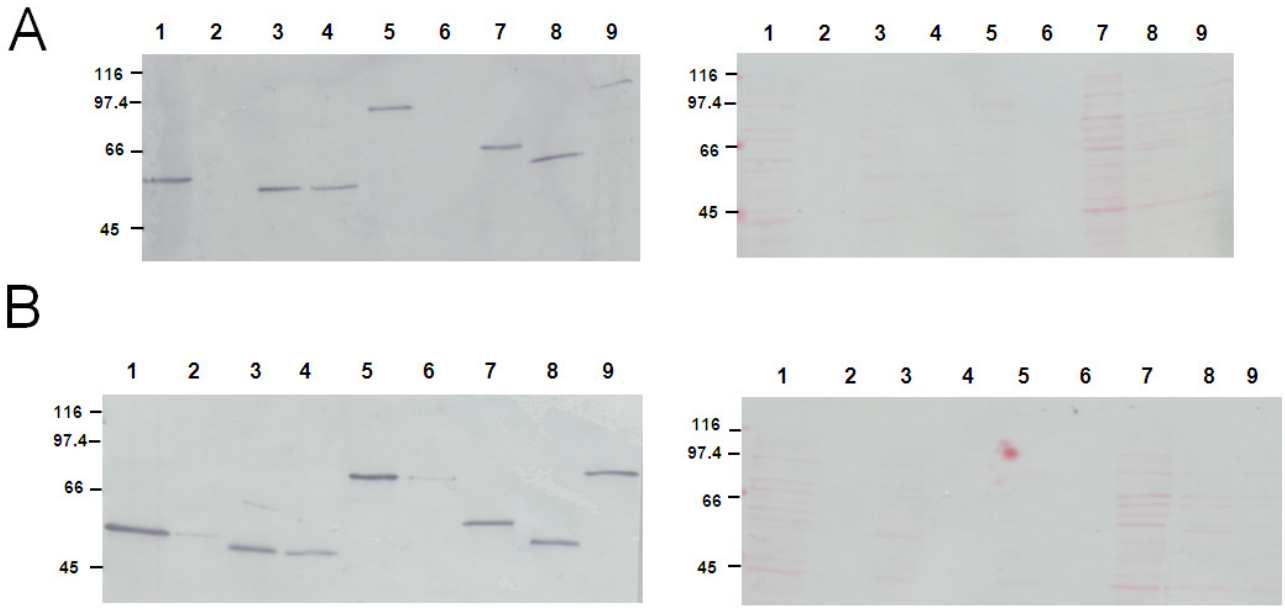

Figure 8 – Western blotting using anti-Histag and anti-AIP56 antibodies. The soluble fraction of induced *E. coli* cultures of chimeras A1 (lane 9), B1 (lane 7), C1 (lane 8) and both flow-through and elution fractions collected in trial-scale purifications of chimeras A2 (lanes 5 and 6, respectively), B2 (lanes 1 and 2, respectively) and C2 (lanes 3 and 4 respectively) were separated in a 12% SDS-PAGE and transferred onto nitrocellulose membrane. **A)** Membrane staining with Ponceau S (right-handed image) and western blotting profile using anti-Histag antibody (left-handed image). **B)** Membrane staining with Ponceau S (right image) and western blotting profile using anti-AIP56 antibody (left image). After incubation with the primary antibodies, membranes were washed and incubated with anti-

rabbit (for AIP56) or anti-mouse (for Histag) alkaline phosphatase conjugate. The presence of the immunoreactive bands was detected with BCIP/NBT. In all lanes, bands with the predicted molecular weight were obtained.

Considering that the low yield in the trial-scale purifications was not due to lack of His-tag in the recombinant proteins, a larger scale purification protocol under native conditions was tested. Protein samples were loaded onto HisTrap chromatography columns and, after binding of the fusion proteins, elution was performed using a 50-250 mM imidazole gradient. Imidazole acts as a competitor ligand for nickel ions and, when used in excess leads to the release and consequent elution of the proteins bound to the column. Although in this case protein elution yield increased substantially (data not shown), protein precipitation was observed after chromatography. In an attempt to increase protein stability, in subsequent purification protocols, imidazole-free buffer was added to the eluted fractions in order to lower protein and imidazole concentrations. Moreover, glycerol was added to all buffers used on the purification process as well as to the lysis buffer. Glycerol is known to act as a stabilizing agent by shifting the native protein ensemble to more compact states and by inhibiting protein aggregation [48]. In order to remove imidazole from purified fusion protein solutions, buffer exchange by desalting was performed. The resulting samples were concentrated using centrifugal devices to the final concentrations presented in table 5.

Table 5 – Concentration of purified protein and their respective predicted molecular weights.

Chimera	Predicted molecular weight (kDa)	Concentration (mg/mL)	Concentration (µM)
A1	85.9	14.41	168
A2	77.7	0.78	10
B1	62.3	2.88	46
B2	54	0.98	18
C1	57	8.76	153
C2	48.9	8.17	167

Purification profiles are shown in figures 9-14. The first peak observed in each chromatogram corresponds to compounds produced by *E.coli* that were weakly bound to the column and eluted at low imidazole concentrations. On the other hand, the second peak of each chromatogram (blue arrow) corresponds to the elution of the respective fusion protein. Interestingly, the highest purification yields were obtained for proteins C1 and C2. The reason for this result is not yet known but a possible explanation can be the higher induction yield observed in these chimeras or, on the other hand, the formation of a more stable structural arrangement of truncate C with both reporter moieties, due to unknown interactions, in comparison to the other chimeras.

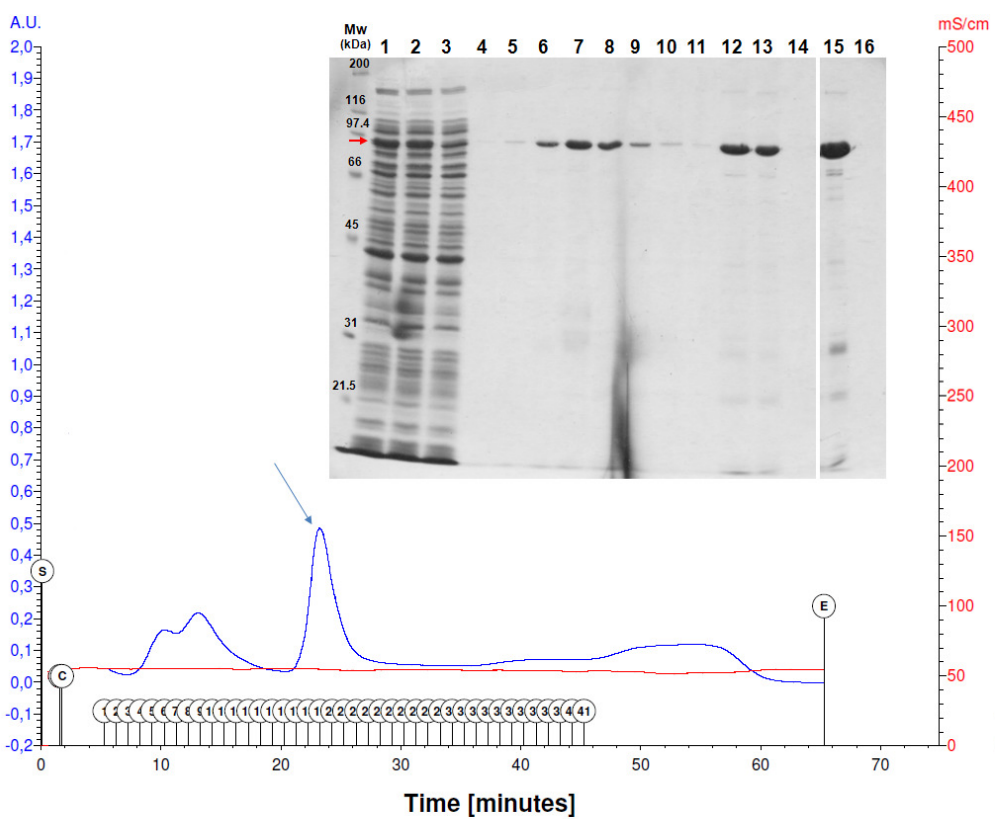

Figure 9 – Purification profile of AIP56 chimera A1. The soluble fraction of induced *E. coli* cultures (lane 1) was filtered with a 0.2 µm filter (lane 2) and applied to HisTrap™ HP column (GE Healthcare). Flow-through fraction (lane 3) was collected. Elution was carried out with step-increasing concentrations of imidazole in 50 mM sodium phosphate buffer pH 7.4 containing 500 mMNaCl and 10% glycerol. Column elutes were monitored for absorbance at 280 nm (blue line in chromatogram). Fractions comprising the peak corresponding to elution of chimera A1 (blue arrow and lanes 4 to 11) were diluted 1:1 (v/v) in imidazole-free buffer and pooled (lane 12). The buffer of the pool was exchanged to 20 mM Tris-HCl pH 8.0, 200 mM NaCl, 5% glycerol by desalting (lane 13). The resulting protein solution was concentrated using centrifugal devices (lane 15). Lane 14: wash fraction from the desalting. Lane 16: Flow-through fraction of concentration. Each lane contains the equivalent to 200 µL bacterial culture, except for lane 15, which contains the equivalent to 400 µL bacterial culture. The position of chimera A1 is indicated by the red arrow. The red line represents the conductivity. The lanes shown are from the same gel and were cut and juxtaposed only for presentation in the figure.

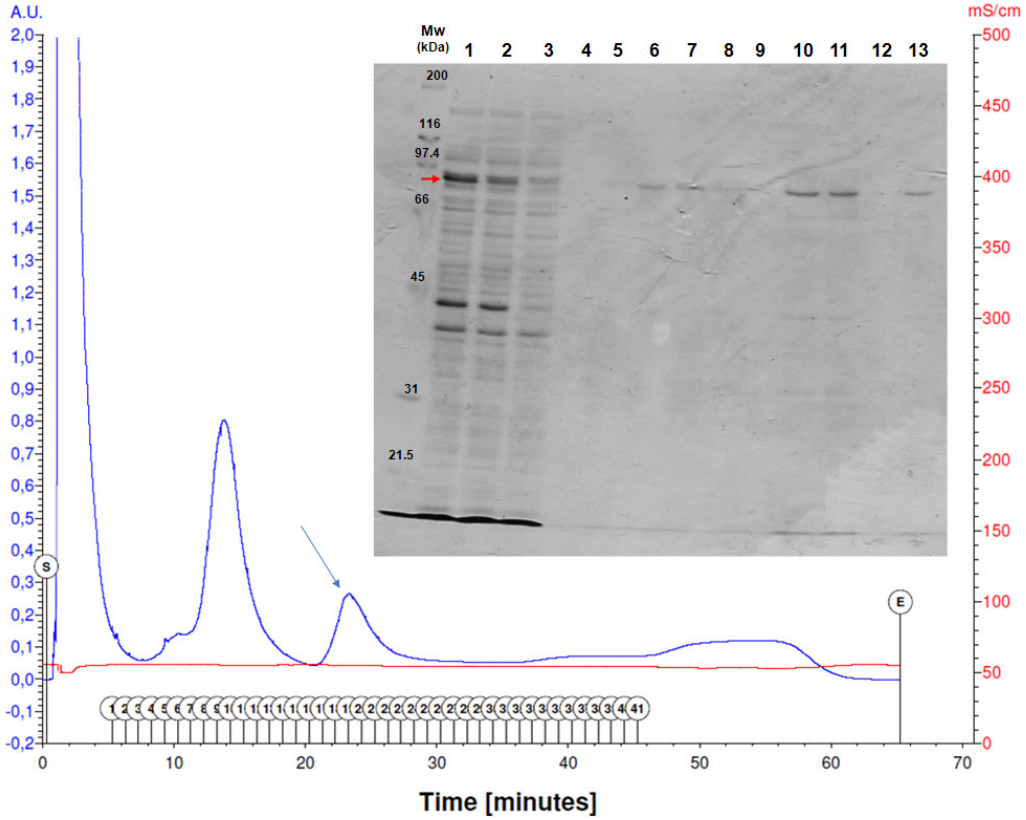

Figure 10 – Purification profile of AIP56 chimera A2. The soluble fraction of induced *E. coli* cultures (lane 1) was filtered with a 0.2 µm filter (lane 2) and applied to HisTrap™ HP column (GE Healthcare). Flow-through fraction (lane 3) was collected. Elution step was carried out with step-increasing concentrations of imidazole in 50 mM sodium phosphate buffer pH 7.4; 500 mMNaCl; 10% glycerol. Column elutes were monitored for absorbance at 280 nm (blue line in chromatogram). Fractions comprising the peak corresponding to elution of chimera A2 (blue arrow and lanes 4 to 9) were diluted 1:1 (v/v) in imidazole-free buffer and pooled (lane 10). The buffer of the pool was exchanged to 20 mM Tris-HCl pH 8.0, 200 mM NaCl, 5% glycerol by desalting (lane 11). The resulting protein solution was concentrated using centrifugal devices (lane 13). Lane 12: Flow-through fraction of concentration. Each lane contains the equivalent to 200 µL bacterial culture. The position of chimera A2 is indicated by the red arrow. The red line represents the conductivity.

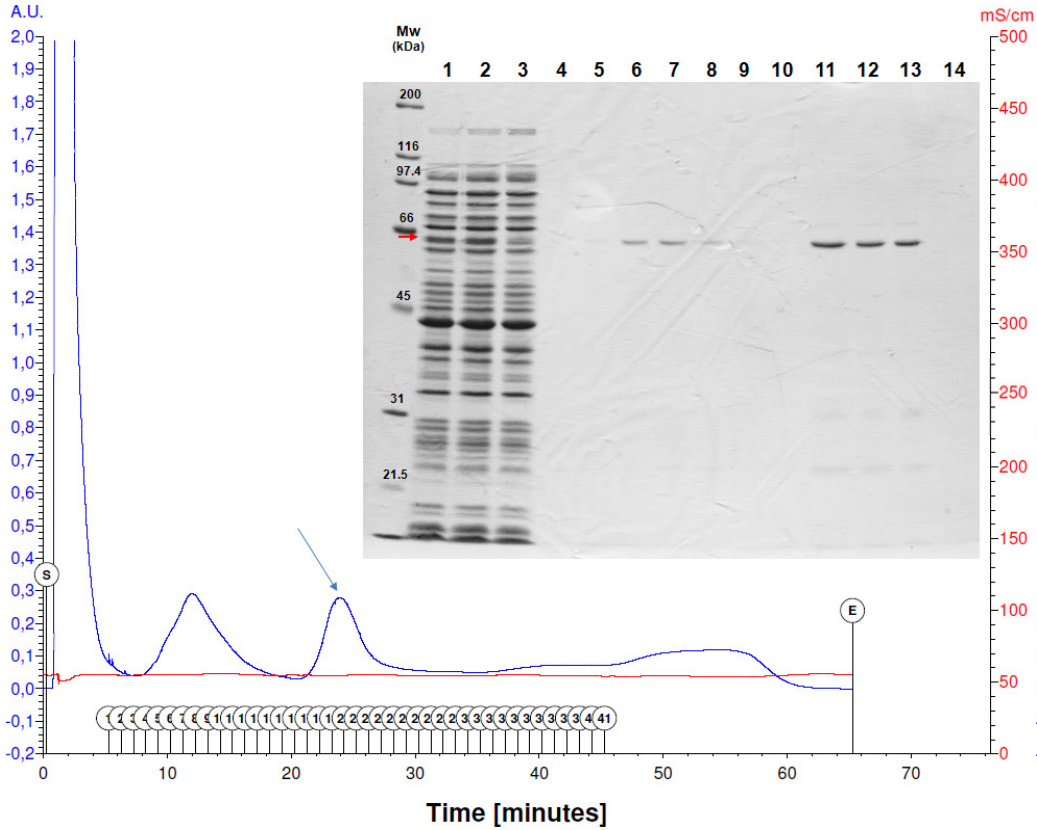

Figure 11 – Purification profile of AIP56 chimera B1. The soluble fraction of induced *E. coli* cultures (lane 1) was filtered with a 0.2 µm filter (lane 2) and applied to HisTrap™ HP column (GE Healthcare). Flow-through fraction (lane 3) was collected. Elution step was carried out with step-increasing concentrations of imidazole in 50 mM sodium phosphate buffer pH 7.4; 500 mM NaCl; 10% glycerol. Column elutes were monitored for absorbance at 280 nm (blue line in chromatogram). Fractions comprising the peak corresponding to elution of chimera B1 (blue arrow and lanes 4 to 10) were diluted 1:1 (v/v) in imidazole-free buffer and pooled (lane 11). The buffer of the pool was exchanged to 20 mM Tris-HCl pH 8.0, 200 mM NaCl, 5% glycerol by desalting (lane 12). The resulting protein solution was concentrated using centrifugal devices (lane 13). Lane 14: Flow-through fraction of concentration. Each lane contains the equivalent to 200 µL bacterial culture. The position of chimera B1 is indicated by the red arrow. The red line represents the conductivity.

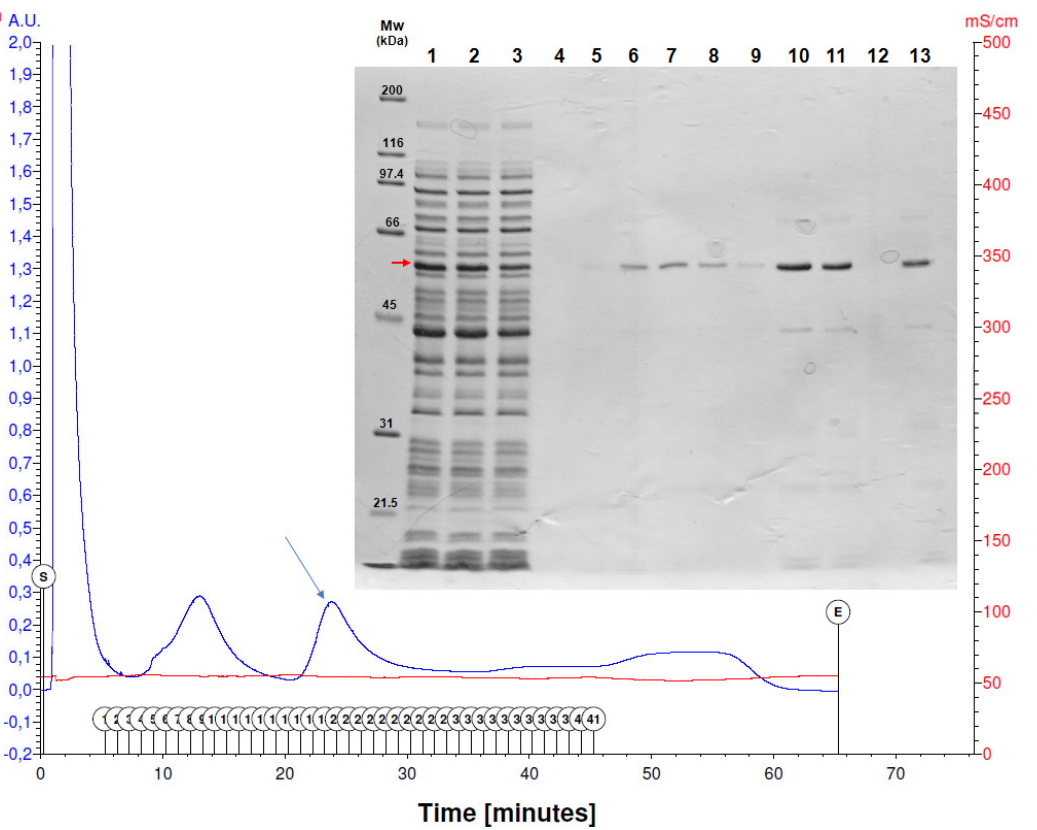

Figure 12 – Purification profile of AIP56 chimera B2. The soluble fraction of induced *E. coli* cultures (lane 1) was filtered with a 0.2 µm filter (lane 2) and applied to HisTrap™ HP column (GE Healthcare). Flow-through fraction (lane 3) was collected. Elution step was carried out with step-increasing concentrations of imidazole in 50 mM sodium phosphate buffer pH 7.4; 500 mM NaCl; 10% glycerol. Column elutes were monitored for absorbance at 280 nm (blue line in chromatogram). Fractions comprising the peak corresponding to elution of chimera B2 (blue arrow and lanes 4 to 9) were diluted 1:1 (v/v) in imidazole-free buffer and pooled (lane 10). The buffer of the pool was exchanged to 20 mM Tris-HCl pH 8.0, 200 mM NaCl, 5% glycerol by desalting (lane 11). The resulting protein solution was concentrated using centrifugal devices (lane 13). Lane 12: Flow-through fraction of concentration. Each lane contains the equivalent to 200 µL bacterial culture. The position of chimera B2 is indicated by the red arrow. The red line represents the conductivity.

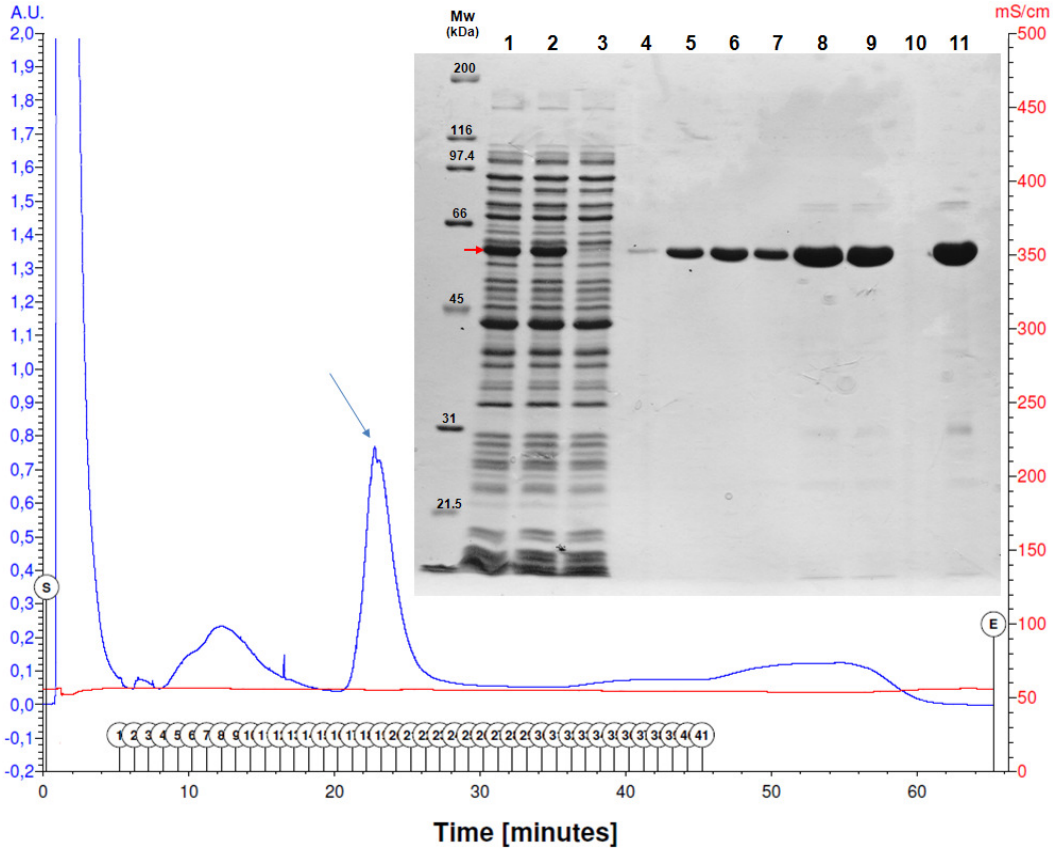

Figure 13 – Purification profile of AIP56 chimera C1. The soluble fraction of induced *E. coli* cultures (lane 1) was filtered with a 0.2 µm filter (lane 2) and applied to HisTrap™ HP column (GE Healthcare). Flow-through fraction (lane 3) was collected. Elution step was carried out with step-increasing concentrations of imidazole in 50 mM sodium phosphate buffer pH 7.4; 500 mM NaCl; 10% glycerol. Column elutes were monitored for absorbance at 280 nm (blue line in chromatogram). Fractions comprising the peak corresponding to elution of chimera C1 (blue arrow and lanes 4 to 7) were diluted 1:1 (v/v) in imidazole-free buffer and pooled (lane 8). The buffer of the pool was exchanged to 20 mM Tris-HCl pH 8.0, 200 mM NaCl, 5% glycerol by desalting (lane 9). The resulting protein solution was concentrated using centrifugal devices (lane 11). Lane 10: Flow-through fraction of concentration. Each lane contains the equivalent to 200 µL bacterial culture, except for lane 11, which contains the equivalent to 400 µL bacterial culture. The position of chimera C1 is indicated by the red arrow. The red line represents the conductivity.

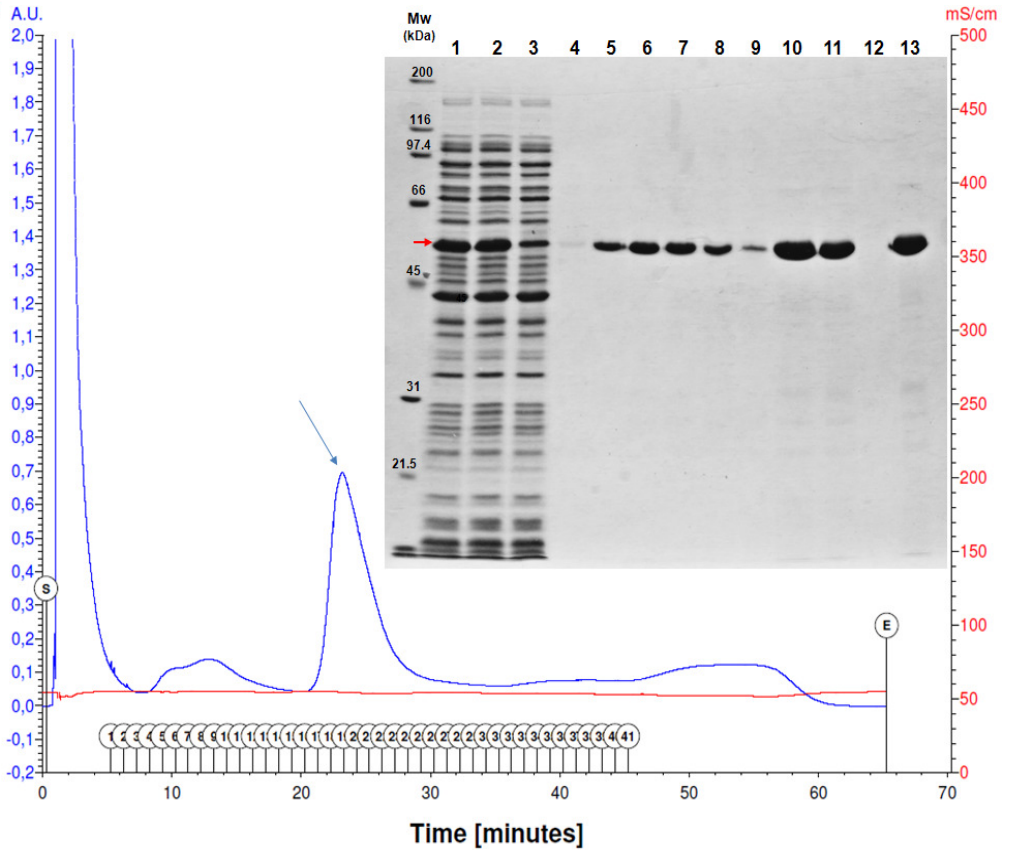

Figure 14 – Purification profile of AIP56 chimera C2. The soluble fraction of induced *E. coli* cultures (lane 1) was filtered with a 0.2 µm filter (lane 2) and applied to HisTrap™ HP column (GE Healthcare). Flow-through fraction (lane 3) was collected. Elution step was carried out with step-increasing concentrations of imidazole in 50 mM sodium phosphate buffer pH 7.4; 500 mM NaCl; 10% glycerol. Column elutes were monitored for absorbance at 280 nm (blue line in chromatogram). Fractions comprising the peak corresponding to elution of chimera C2 (blue arrow and lanes 4 to 9) were diluted 1:1 (v/v) in imidazole-free buffer and pooled (lane 10). The buffer of the pool was exchanged to 20 mM Tris-HCl pH 8.0, 200 mM NaCl, 5% glycerol by desalting (lane 11). The resulting protein solution was concentrated using centrifugal devices (lane 13). Lane 12: Flow-through fraction of concentration. Each lane contains the equivalent to 200 µL bacterial culture, except for lane 13, which contains the equivalent to 400 µL bacterial culture. The position of chimera C2 is indicated by the red arrow. The red line represents the conductivity.

C. Evaluation of the enzymatic activity of the fusion proteins

After purification of the fusion proteins, the next stage was the evaluation of their enzymatic activity. Due to the fact that the primary goal for the development of these chimeras is their use in intoxication assays, aiming at identifying the AIP56 binding/internalization domain, it is extremely important to confirm that they are enzymatically active, to be able to use their enzymatic activity as a readout for internalization.

In the case of β-lactamase-containing chimeras, the enzymatic activity was tested using nitrocefin as a substrate. Nitrocefin is a chromogenic cephalosporin that undergoes a rapid distinctive colour change from yellow (λ= 390 nm) to red (λ= 486 nm) when hydrolysed, in the beta-lactam ring, by β-lactamase [49]. This substrate provides an easy and rapid method of enzymatic detection of β-lactamase. The fusion proteins A1, B1 and C1 were incubated with nitrocefin at 30 ºC for 1 h and the emission at 390 nm and 486 nm for each reaction was measured every minute. For this experience, a negative control (nitrocefin only) and a positive control (crude β-lactamase extract, obtained from *E.coli* cells carrying the plasmid pET-23b(+) were also used. After 5 minutes incubation, both positive control (figure 15A) and chimeras A1, B1 and C1 (figure 15B) exhibited an increase in absorbance at 486 nm (cleaved nitrocefin), whereas the absorbance at 390 nm (intact nitrocefin) has suffered a decrease. On the other hand, after the same incubation time, no alteration was observed in both absorbances (390 nm and 486 nm) for the negative control (figure15 A), meaning that nitrocefin was not cleaved in this situation. Altogether, these results reflect the presence of β-lactamase activity in all three chimeras tested.

The enzymatic activity of the Dta moiety in Dta-containing chimeras was detected by testing their ability to inhibit protein synthesis *in vitro*. It is well established that DT, through its A moiety, inhibits protein synthesis by transfer of an ADP-ribose moiety from NAD^+ onto EF-2 [8]. Consequently, the presence of DTa, in its active state, during protein synthesis prevents protein elongation by blocking the incorporation of amino acids. Thus, it is possible to evaluate the DTa activity by assessing its ability to inhibit the incorporation of radioactive amino-acids in a protein synthesis assay *in vitro*. In the present work, a highly efficient *in vitro* eukaryotic protein synthesis system based on rabbit reticulocyte lysate was used. Reticulocytes (immature erythrocytes) are highly specialized cells, primarily responsible for the synthesis of hemoglobin, that, despite of the lack of cell nucleus, contain the cellular components necessary for protein synthesis (transfer RNA (ribonucleic acid), ribosomes, amino acids, initiation, elongation and termination factors) [50]. The readout used for this experiment was the detection, by autoradiography, of newly synthesized proteins containing radioactive amino acids, incorporated during the translation process. For this purpose, rabbit reticulocyte lysates were supplemented with NAD^+ (ADP moiety donor in ADP-rybosilation mediated by DTa) and pre-incubated with all the additives previously described in chapter II(section F) before adding the fusion proteins. Lysate only and lysate supplemented with

NAD+ or NAD+ plus chimera A1 (a chimera containing the β-lactamase moiety as reporter and, therefore, not able to inhibit protein synthesis) were used as negative controls. DT and ciclohexamide, a known protein synthesis inhibitor that blocks the translocation step in enlogation [51], as positive controls.

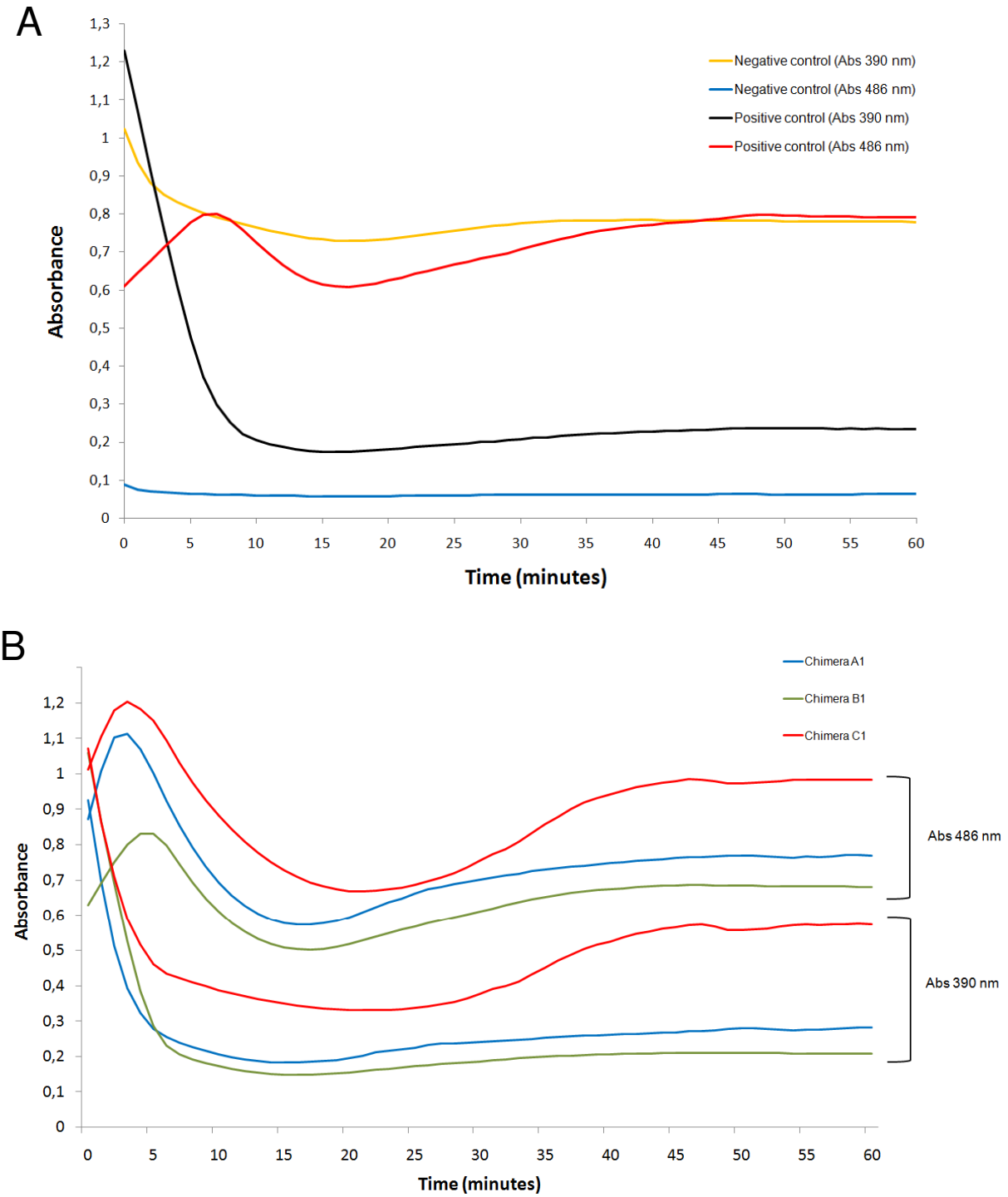

Figure 15 – Detection of β-lactamase activity in chimeras A1, B1 and C1. Purified protein samples were incubated with nitrocefin for 1 h at 30ºC in a luminescence microplatereader and the microplate wells absorbance was read, every minute, at 390nm and 486nm. **A)** Negative (90 µL 100 mM sodium phosphate buffer pH 7.0 + 10 µL 0.4 mM nitrocefin) and positive (82 µL 100 mM sodium phosphate buffer pH 7.0 + 8 µL crude β-lactamase extract + 10 µL 0.4 mM nitrocefin) controls activity profile. **B)** β-lactamase activity profile of

chimeras A1, B1 and C1 (82 µL 100 mM sodium phosphate buffer pH 7.0 + 8 µL purified fusion protein (A1, B1 or C1) + 10 µL 0.4 mM nitrocefin). All values were obtained in comparison to blank well (90 µL 100 mM sodium phosphate buffer pH 7.0 + 10 µL DMSO).

Following unpublished evidences from our laboratory, showing that AIP56 inhibits protein synthesis in intoxicated cells, we also tested this toxin. Afterwards, plasmid encoding p65RelA and [^{35}S] methionine were added to each condition and incubated for 90 min at 30ºC. Samples were subjected to SDS-PAGE and afterwards transferred onto a nitrocellulose membrane. The radioactive bands were detected by autoradiography. As shown in figure 16, a band with the expected molecular weight, corresponding to p65, was obtained in untreated lysates as well as in lysates supplemented with NAD+ or NAD+ plus chimera A1. In contrast, this band was absent when the lysates were pre-incubated with the fusion proteins A2, B2 and C2, in both concentrations tested (0.04 and 0.004 µg/µL), as well as in the positive controls (DT and ciclohexamide). This indicates that protein synthesis was inhibited by fusion proteins A2, B2 and C2. In accordance to what was observed in previous studies in our laboratory, protein synthesis was also inhibited by AIP56, through a process still undisclosed. Altogether, these results confirm that the DTa reporter in chimeras A2, B2 and C2 is catalytically active.

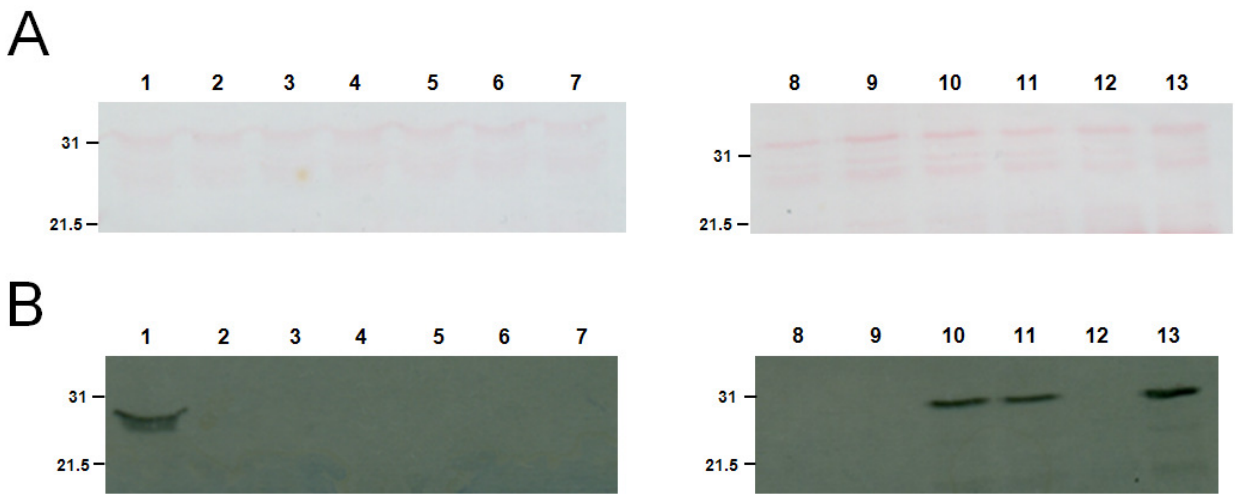

Figure 16 – Detection of DTa activity in chimeras A2, B2 and C2. In this experiment, an end point activity assay was performed. ADP-rybosilation of EF-2 by DTa moiety was assessed by the incorporation of [^{35}S] methionine during NF-kB p65 subunit synthesis. Erythrocyte rabbit lysates supplemented with 1 µg/uL NAD+ were pre-incubated for 10 min at 30 ºC with the following additives: lysate only (without additives; lane 1); NAD^+ (lane13); 1 µg or 0.1 µg of purified chimera A1 (lane 10 and 11 respectively); DT (lane 3); ciclohexamide (lane 12); AIP56 (lane 2); 1 µg or 0.1 µg of purified chimera A2 (lane 8 and 9 respectively); 1 µg or 0.1 µg of purified chimera B2 (lane 4 and 5 respectively); 1 µg or 0.1 µg of purified chimera C2 (lane 6 and 7 respectively). Afterwards p65RelA containing plasmid and [^{35}S] methionine were added and the mixtures incubated for 90 min at 30ºC. SDS-PAGE gel containing the resulting reaction products was transferred to a nitrocellulose membrane. Staining with Ponceau S (**A**) and film exposed for 48h to the membrane (**B**) are shown.

D. Determination of the optimal conditions for β-lactamase substrate loading into mBMDMs

Following the confirmation that all chimeras possessed enzymatic activity, preliminary experiments aiming at optimizing the conditions for *in vivo* studies with β-lactamase-AIP56 chimeras (A1, B1 and C1) were performed. For this purpose, the loading of the β-lactamase substrate CCF4-AM into mBMDMs was evaluated, following the protocol described in chapter II (section H). In this screening, incubation with the substrate was carried out until 4 h, and emitted fluorescence analyzed at different time points using an inverted epifluorescence microscope. The development of FRET from the intact substrate (green fluorescence signal; emission at 520 nm) within mBMDMs was clearly observed at 30 min of incubation (data not show). Notably, all cells were emitting green fluorescence indicating that the CCF4 had already reached the cytosol at this early time point. Fluorescence was equally detected at later time points (until 4h). This outcome not only elucidates about the loading efficiency under the conditions used, but also provides information on the incubation time necessary for the visualization of the substrate inside the cells. Hence, time saving protocols can be implemented.

E. Intoxication assays of mBMDM with β-lactamase-AIP56 chimeras

The next and final step of this project was to test the ability of the chimeras to translocate their respective reporter moieties into the cytosol of mBMDM. In the case of β-lactamase containing chimeras (A1, B1 and C1), this evaluation was performed by incubating the cells with the chimeras, followed by incubation with the β-lactamase substrate CCF4-AM and subsequent detection of FRET disruption. As previously described, CCF4-AM performs FRET through its two fluorophores, and upon cleavage mediated by the reporter moiety, the emission wavelength of this molecule is shifted. This change allows tracking the arrival of β-lactamase at the cytosol. In this assay, mBMDM were incubated for 1 h at 37 ºC with either chimeras A1, B1 and C1 or chimeras A2, B2 and C2 (used as negative controls) or with the chimera LFnBla. In the case of the last chimeric protein, its ability to translocate to the cytosol and cleave β-lactamase substrates that perform FRET was already proven [31] and, therefore, LFnBla was used as the positive control of this experiment. Following this step, mBMDMs were incubated for 30 min with CCF4 and the fluorescence emitted by the intact or cleaved substrate was observed and evaluated by microscopy. As seen in figure 17, chimeras B1, A1 and the positive control show the highest value of FRET disruption, indicating that in these 3 conditions the β-lactamase moiety was efficiently translocated into the cytosol. On the other hand, chimera C1 and all DTa containing chimeras displayed FRET disruption values similar to the negative control (mBMDM incubated only with the

substrate), showing that chimera C1 was not able to translocate its reporter moiety to the cytosol.

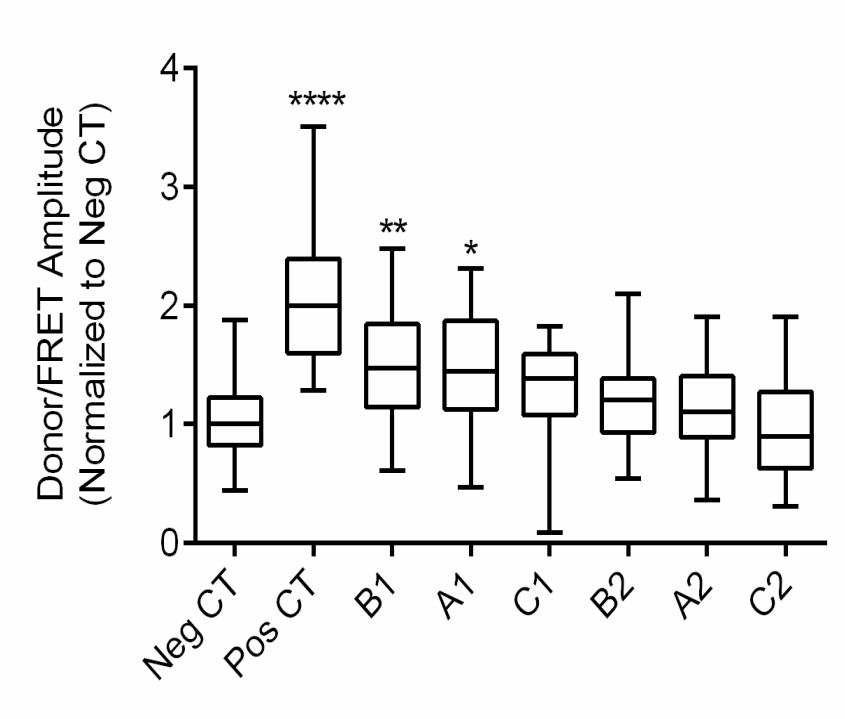

Figure 17 – Detection of FRET disruption in mBMDM incubated with β-lactamase-AIP56 chimeras. mBMDM were first incubated with the chimeras for 1 h at 37 ºC followed by medium wash with PBS 1x. After this step, the cells were incubated for 30 min at RT with standard CCF4 loading solution and the FRET disruption was observed using an inverted epifluorescence microscope.

F. Preliminary intoxication assays of mBMDM with DTa-AIP56 chimeras

Regarding the DTa containing chimeras (A2, B2 and C2), only preliminary *in vivo* assays were performed. In these tests, mBMDMs were incubated with the chimeras, positive controls (DT and cicloheximide) or AIP56 (either wild-type or catalytically inactive toxin) for 16 h at 37 ºC. Following this step, the mBMDM's medium was removed and the cells were incubated with a medium containing radioactive methionine for 1 h at 37 ºC. After protein precipitation, radioactive aminoacid incorporation was measured by scintillation counting. The results of this assay are shown in figure 18. As expected, both positive controls (DT and cicloheximide) possess the lowest values of [^{35}S] methionine incorporation, which translates in the highest values of protein translation inhibition. A similar incorporation, and therefore, inhibition value is observed for chimera B2. This result reflects the successful translocation of the DTa moiety mediated by this chimera and the consequently activity of this reporter in the cytosol of mBMDM. In contrast, both A2 and C2 chimeras show incorporation values similar to the mock condition, which means that protein

translation was not inhibited and, therefore, translocation of DTa was impaired. The results obtained for chimeras B2 and C2 are in agreement with the outcome observed in the assays with the β-lactamase-AIP56 chimeras and emphasize the importance of the region present in AIP56 truncate B (but absent in truncate C) for the correct translocation of the toxin to the cytosol of cells.

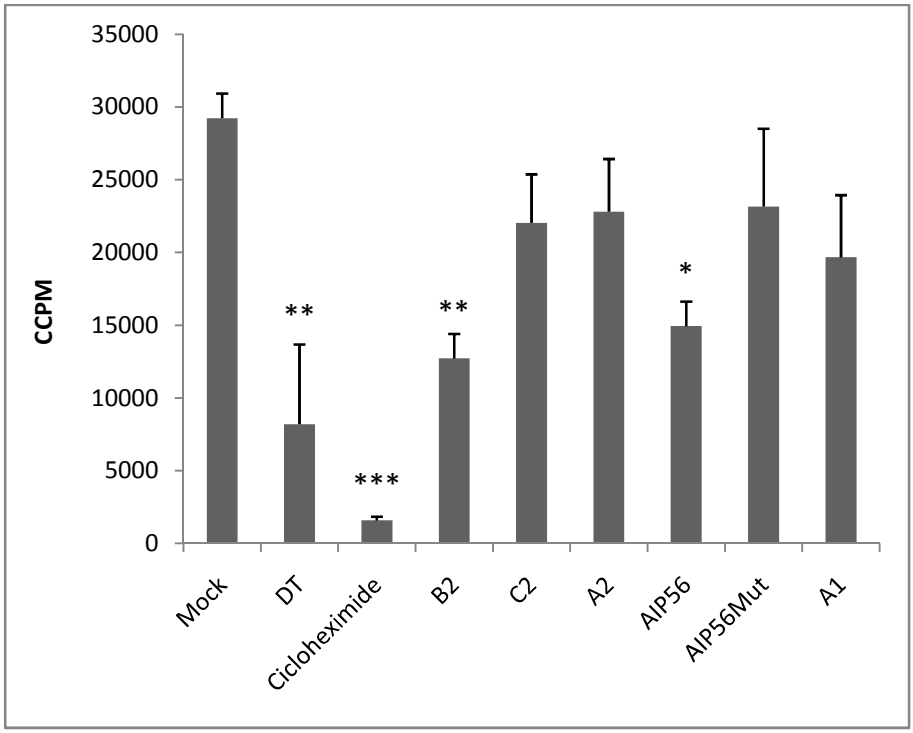

Figure 18– Detection of [^{35}S] methionine incorporation in mBMDM translation process upon incubation with AIP56 chimeras. mBMDM were first incubated with the chimeras for 16 h at 37 ºC followed by medium removal and exchange with a medium containing radioactive methionine. After incubation of the cells with this medium for 1 h at 37 ºC and protein precipitation, radioactive aminoacid incorporation was measured by scintillation counting. CCPM = corrected counts *per* minute.

Chapter IV:
Conclusion

Phdp is the causative agent of a deadly septicaemic infection affecting economically important marine fish species. Due to this fact, the search for ways to prevent the disease caused by this pathogen is imperative. In order to develop preventive strategies it is essential to unveil and understand the virulence mechanisms used by the pathogen to cause host infection. In 2005, a novel virulence factor of *Phdp* was discovered: AIP56 [29]. This bacterial protein is now recognized as the main factor for the pathogen's success and its characterization has already provided key insights to the understanding of the pathogenesis of infection by *Phdp* [29, 31]. Several studies have been conducted throughout the last years with the objective of enlighten the structural features of AIP56. Despite this effort, the exact steps followed by AIP56 during its intoxication process are not yet fully understood. Prediction of secondary structures together with limited proteolysis assays confirmed that AIP56 is organized into two structural domains: a N-terminal catalytic domain and a C-terminal binding/translocation domain [31]. Despite this classification, there are still not definitive evidences that the C-terminal domain alone is responsible for the AIP56 translocation process. Recently, the ability of AIP56 C-terminus ($AIP56^{251-497}$) to deliver the NleC catalytic region into cells was tested [31]. In this work, the authors replaced the AIP56 N-terminal region ($AIP56^{1-250}$) by$NleC^{1-270}$, leading to the production of the chimera $NleC^{1-270}$-$AIP56^{251-497}$. Upon incubation of this chimera with cells, no p65 cleavage was observed, which could possibly be justified by an inefficient delivery into cytosol. Moreover, this failure could be explained by the fact that NleC is directly injected into the cell cytosol by its producing bacteria through a type III secretion system [52] and, therefore, may not have the ability/requirements to undergo internalization and translocation through the AIP56 mechanism. On the other hand, considering that the exact boundaries of AIP56 binding/translocation domain were not yet established, an important region of the toxin could have also been omitted upon design of this chimera. AIP56 secondary structure analysis has shown the presence of a potentially important region for the translocation process, upstream of the AIP56 C-terminal region used for the previous chimera, corresponding to amino 210 to 256. This region contains a decapeptide similar to the conserved T1 motif reported for other AB toxins [8], as well as a region, immediately prior to this decapeptide, comprised of a predicted helix and an amphipathic helix [31]. The T1 motif, and adjacent lysine residues in transmembrane helix 1, have been reported to play an important role in the DTa entry in cell cytosol by binding to the COPI (coat protein complex), a complex known to facilitate endossomal vesicular trafficking and the retrograde transport of vesicles between Golgi compartments [8, 53, 54]. Based on all facts mentioned above, the aim of this project was the development of molecular tools that could be used in future studies aiming at evaluating whether this region could play a crucial role in the binding/translocation mechanism of AIP56 into cells.

All six chimeras designed for this study were successfully produced and purified, despite all the drawbacks encountered during these processes. Furthermore, the enzymatic activities of the

reporter moieties were also tested. In all cases, the reporter domain has shown to be catalytically active. The next, and final, step of this project was the test of these chimeras in cells, more specifically mBMDM, previously used in AIP56 studies. Protocol optimization of this experiment was performed for the β-lactamase-AIP56 chimeras and preliminary assays using the DTa-AIP56 chimeras were also conducted.In both experiments, a similar result was obtained: the AIP56 truncate B, comprising the T1-like motif and the two predicted helices, was able to translocate the two reporter moieties used in this study, whereas the AIP56 truncate C lacked the ability to transport either β-lactamase or DTa to the cytosol. Taking into consideration this outcome, we can conclude that the AIP56 region present in the truncate B but absent in truncate C is required for the efficient delivery of this toxin into the cytosol of cells. Of note is also the outcome observed for the AIP56 full length mutant (region A). Even though this region successfully delivered the β-lactamase to the cytosol, the same result did not happened in the case of the DTa moiety. The structural/interaction incompatibilities between this reporter moiety and the AIP56 full length mutant or the fact that these assays are only preliminary and require more specific conditions can be considered as possible reasons for the absence of translocation in this particular case. Despite this fact, the importance of the region comprising the T1-like motif and the two predicted helices for the delivery of the toxin was proven in this study, as well as, the ability of the AIP56 toxin to transport other non-permeable proteins to the intracellular compartment.

The understanding of the role played by the region encompassing the T1-like motif and the predicted helices for AIP56 intoxication vastly contributes for the definition of the boundaries of AIP56 binding/translocation domain. Consequently, this discovery will also improve the understanding of the toxin structure/function relationships and interaction with cells.

Given the already greatly explored potential of some AB toxins as therapeutic agents as well as tools in cell biology studies, it is reasonable to think that AIP56 could also be used for the same purposes. Due to its reported ability to target NF-kB, whose uncontrolled activation is often seen in multiple inflammatory, autoimmune and cancer diseases [55], in addition to its intrinsic ability to reach the cytosol of target cells, it is clear that this toxin shares the same or even greater potential to become a therapeutic agent. In addition, AIP56 might also be a valuable tool in cell biology studies, particularly in the study of the molecular details of the NF-κB-mediated regulation of apoptosis and inflammation processes. However this potential can only be fulfilled with in depth knowledge about the toxin structure/function relationship as well as about its intoxication mechanism.

Chapter V:

References

1. Yersin, É.R.A., *Contribution à l'étude de la diphtérie*, ed. I. Pasteur. Vol. 12. 1889. 42.
2. Peterson, J., *Bacterial Pathogenesis*, in *Medical Microbiology.*, e. Baron S, Editor. 1996: Galveston (TX): University of Texas Medical Branch at Galveston.
3. Henkel, J.S., M.R. Baldwin, and J.T. Barbieri, *Toxins from bacteria.*EXS, 2010. **100**: p. 1-29.
4. Popoff, M.R., *Bacterial exotoxins.* Contrib Microbiol, 2005. **12**: p. 28-54.
5. Lemichez, E. and J.T. Barbieri, *General aspects and recent advances on bacterial protein toxins.* Cold Spring Harb Perspect Med, 2013. **3**(2): p. a013573.
6. Odumosu, O., et al., *AB toxins: a paradigm switch from deadly to desirable*, in *Toxins (Basel)*. 2010. p. 1612-45.
7. *Programa Nacional de Vacinação*. Available from: http://www.portaldasaude.pt/portal/conteudos/informacoes+uteis/vacinacao/vacinas.htm.
8. Murphy, J.R., *Mechanism of diphtheria toxin catalytic domain delivery to the eukaryotic cell cytosol and the cellular factors that directly participate in the process.* Toxins (Basel), 2011. **3**(3): p. 294-308.
9. Becker, N.B., I., *Antibody-Based Immunotoxins for the Treatment of Cancer.* Antibodies, 2012. **1**: p. 39-69.
10. Wilson, J.W., et al., *Mechanisms of bacterial pathogenicity.* Postgrad Med J, 2002. **78**(918): p. 216-24.
11. Jianjun, S., *Roles of Cellular Redox Factors in Pathogen and Toxin Entry in the Endocytic Pathways.* In Molecular Regulation of Endocytosis, 2012.
12. Falnes, P.O. and K. Sandvig, *Penetration of protein toxins into cells.* Curr Opin Cell Biol, 2000. **12**: p. 407-413.
13. Beddoe, T., et al., *Structure, biological functions and applications of the AB5 toxins.* Trends Biochem Sci, 2010. **35**(7): p. 411-8.
14. Bann, J.G., *Anthrax toxin protective antigen--insights into molecular switching from prepore to pore.* Protein Sci, 2012. **21**(1): p. 1-12.
15. Montecucco, C., E. Papini, and G. Schiavo, *Bacterial protein toxins penetrate cells via a four-step mechanism.* FEBS Lett, 1994. **346**(1): p. 92-8.
16. Sandvig, K., et al., *Pathways followed by protein toxins into cells.* International Journal of Medical Microbiology, 2004. **293**(7-8): p. 483-490.
17. Kagan, B.L., A. Finkelstein, and M. Colombini, *Diphtheria toxin fragment forms large pores in phospholipid bilayer membranes.* Proc Natl Acad Sci U S A, 1981. **78**(8): p. 4950-4.
18. Donovan, J.J., et al., *Diphtheria toxin forms transmembrane channels in planar lipid bilayers.* Proc Natl Acad Sci U S A, 1981. **78**(1): p. 172-6.
19. Collier, R.J., *Understanding the mode of action of diphtheria toxin: a perspective on progress during the 20th century.* Toxicon, 2001. **39**(11): p. 1793-803.

20. Greenfield, L., et al., *Nucleotide sequence of the structural gene for diphtheria toxin carried by corynebacteriophage beta.* Proc Natl Acad Sci U S A, 1983. **80**(22): p. 6853-7.
21. Bennett, M.J., S. Choe, and D. Eisenberg, *Refined structure of dimeric diphtheria toxin at 2.0 A resolution.* Protein Sci, 1994. **3**(9): p. 1444-63.
22. Naglich, J.G., et al., *Expression cloning of a diphtheria toxin receptor: identity with a heparin-binding EGF-like growth factor precursor.* Cell, 1992. **69**(6): p. 1051-61.
23. Moya, M., et al., *Inhibition of coated pit formation in Hep2 cells blocks the cytotoxicity of diphtheria toxin but not that of ricin toxin.* J Cell Biol, 1985. **101**(2): p. 548-59.
24. Kochi, S.K. and R.J. Collier, *DNA fragmentation and cytolysis in U937 cells treated with diphtheria toxin or other inhibitors of protein synthesis.* Exp Cell Res, 1993. **208**(1): p. 296-302.
25. Wernick, N.L., et al., *Cholera toxin: an intracellular journey into the cytosol by way of the endoplasmic reticulum.* Toxins (Basel), 2010. **2**(3): p. 310-25.
26. Fujinaga, Y., et al., *Gangliosides that associate with lipid rafts mediate transport of cholera and related toxins from the plasma membrane to endoplasmic reticulm.* Mol Biol Cell, 2003. **14**(12): p. 4783-93.
27. Feng, Y., et al., *Retrograde transport of cholera toxin from the plasma membrane to the endoplasmic reticulum requires the trans-Golgi network but not the Golgi apparatus in Exo2-treated cells.* EMBO Rep, 2004. **5**(6): p. 596-601.
28. Brunger, A.T., R. Jin, and M.A. Breidenbach, *Highly specific interactions between botulinum neurotoxins and synaptic vesicle proteins.* Cell Mol Life Sci, 2008. **65**(15): p. 2296-306.
29. do Vale, A., et al., *AIP56, a novel plasmid-encoded virulence factor of Photobacterium damselae subsp. piscicida with apoptogenic activity against sea bass macrophages and neutrophils.* Mol Microbiol, 2005. **58**(4): p. 1025-38.
30. Snieszko, S.F., et al., *Pasteurella sp. from an epizootic of white perch (roccus americanus) in chesapeake bay tidewater areas.*J Bacteriol, 1964. **88**: p. 1814-5.
31. Silva, D.S., et al., *The apoptogenic toxin AIP56 is a metalloprotease A-B toxin that cleaves NF-kappab P65.* PLoS Pathog, 2013. **9**(2): p. e1003128.
32. Schiavo, G., et al., *Tetanus toxin is a zinc protein and its inhibition of neurotransmitter release and protease activity depend on zinc.* EMBO J, 1992. **11**(10): p. 3577-83.
33. Hoffmann, A., G. Natoli, and G. Ghosh, *Transcriptional regulation via the NF-kappaB signaling module.*Oncogene, 2006. **25**(51): p. 6706-16.
34. Silva, M.T., N.M. Dos Santos, and A. do Vale, *AIP56: a novel bacterial apoptogenic toxin.*Toxins (Basel), 2010. **2**(4): p. 905-18.
35. Schiavo, G., M. Matteoli, and C. Montecucco, *Neurotoxins affecting neuroexocytosis.* Physiol Rev, 2000. **80**(2): p. 717-66.
36. Costa-Ramos, C., et al., *The bacterial exotoxin AIP56 induces fish macrophage and*

neutrophil apoptosis using mechanisms of the extrinsic and intrinsic pathways. Fish Shellfish Immunol, 2011. **30**(1): p. 173-81.

37. Sandvig, K. and S. Olsnes, *Rapid entry of nicked diphtheria toxin into cells at low pH. Characterization of the entry process and effects of low pH on the toxin molecule.* J Biol Chem, 1981. **256**(17): p. 9068-76.
38. Schiavo, G., et al., *An intact interchain disulfide bond is required for the neurotoxicity of tetanus toxin.* Infect Immun, 1990. **58**(12): p. 4136-41.
39. Romalde, J.L., *Photobacterium damselae subsp. piscicida: an integrated view of a bacterial fish pathogen.* Int Microbiol, 2002. **5**(1): p. 3-9.
40. do Vale, A., F. Marques, and M.T. Silva, *Apoptosis of sea bass (Dicentrarchus labrax L.) neutrophils and macrophages induced by experimental infection with Photobacterium damselae subsp. piscicida.* Fish Shellfish Immunol, 2003. **15**(2): p. 129-44.
41. Silva, M.T., A. do Vale, and N.M. dos Santos, *Secondary necrosis in multicellular animals: an outcome of apoptosis with pathogenic implications.* Apoptosis, 2008. **13**(4): p. 463-82.
42. do Vale, A., et al., *Systemic macrophage and neutrophil destruction by secondary necrosis induced by a bacterial exotoxin in a Gram-negative septicaemia.* Cell Microbiol, 2007. **9**(4): p. 988-1003.
43. Hobson, J.P., et al., *Imaging specific cell surface protease activity in living cells using reengineered bacterial cytotoxins.* Methods Mol Biol, 2009. **539**: p. 115-29.
44. Laemmli, U.K., *Cleavage of structural proteins during the assembly of the head of bacteriophage T4.* Nature, 1970. **227**(5259): p. 680-5.
45. Qureshi, S.A., *Beta-lactamase: an ideal reporter system for monitoring gene expression in live eukaryotic cells.* Biotechniques, 2007. **42**(1): p. 91-6.
46. Hu, H. and S.H. Leppla, *Anthrax toxin uptake by primary immune cells as determined with a lethal factor-beta-lactamase fusion protein.* PLoS One, 2009. **4**(11): p. e7946.
47. Bergmann, S., et al., *Pasteurella multocida toxin as a transporter of non-cell-permeating proteins.* Infect Immun, 2013. **81**(7): p. 2459-67.
48. Vagenende, V., M.G. Yap, and B.L. Trout, *Mechanisms of protein stabilization and prevention of protein aggregation by glycerol.* Biochemistry, 2009. **48**(46): p. 11084-96.
49. O'Callaghan, C.H., et al., *Novel method for detection of beta-lactamases by using a chromogenic cephalosporin substrate.* Antimicrob Agents Chemother, 1972. **1**(4): p. 283-8.
50. *The Basics: In Vitro Translation*. Available from: http://www.lifetechnologies.com/pt/en/home/references/ambion-tech-support/large-scale-transcription/general-articles/the-basics-in-vitro-translation.html.
51. Schneider-Poetsch, T., et al., *Inhibition of eukaryotic translation elongation by cycloheximide and lactimidomycin.* Nat Chem Biol, 2010. **6**(3): p. 209-217.
52. Galan, J.E. and H. Wolf-Watz, *Protein delivery into eukaryotic cells by type III secretion*

machines. Nature, 2006. **444**(7119): p. 567-73.

53. Trujillo, C., et al., *Essential lysine residues within transmembrane helix 1 of diphtheria toxin facilitate COPI binding and catalytic domain entry.* Mol Microbiol, 2010. **76**(4): p. 1010-9.
54. Whitney, J.A., et al., *Cytoplasmic coat proteins involved in endosome function.* Cell, 1995. **83**(5): p. 703-13.
55. DiDonato, J.A., F. Mercurio, and M. Karin, *NF-kappaB and the link between inflammation and cancer.*Immunol Rev, 2012. **246**(1): p. 379-400.